

Neutrinos from the Sun: experimental results confronted with solar models

V. Castellani⁽¹⁾, S. Degl'Innocenti^(2,3), G. Fiorentini^(2,3), M. Lissia⁽⁴⁾ and B. Ricci^(3,5)

⁽¹⁾*Dipartimento di Fisica dell'Università di Pisa, I-56100 Pisa,
Osservatorio Astronomico di Collurania, I-64100 Teramo, and Università dell'Aquila, I-67100
L'Aquila*

⁽²⁾*Dipartimento di Fisica dell'Università di Ferrara, I-44100 Ferrara*

⁽³⁾*Istituto Nazionale di Fisica Nucleare, Sezione di Ferrara, I-44100 Ferrara*

⁽⁴⁾*Dipartimento di Fisica dell'Università di Cagliari, I-09100 Cagliari,
and Istituto Nazionale di Fisica Nucleare, Sezione di Cagliari, I-09100 Cagliari*

⁽⁵⁾*Scuola di Dottorato dell'Università di Padova, I-35100 Padova.*

(July 9, 2021)

Abstract

For standard neutrinos, recent solar neutrino results together with the assumption of a nuclearly powered Sun imply severe constraints on the individual components of the total neutrino flux: $\Phi_{\text{Be}} \leq 0.7 \times 10^9 \text{cm}^{-2}\text{s}^{-1}$, $\Phi_{\text{CNO}} \leq 0.6 \times 10^9 \text{cm}^{-2}\text{s}^{-1}$, and $64 \times 10^9 \text{cm}^{-2}\text{s}^{-1} \leq \Phi_{pp+pep} \leq 65 \times 10^9 \text{cm}^{-2}\text{s}^{-1}$ (at 1σ level). The bound on Φ_{Be} is in strong disagreement with the standard solar model (SSM) prediction $\Phi_{\text{Be}}^{\text{SSM}} \approx 5 \times 10^9 \text{cm}^{-2}\text{s}^{-1}$. We study a large variety of non-standard solar models with low inner temperature, finding that the temperature profiles $T(m)$ follow the homology relationship: $T(m) = kT^{\text{SSM}}(m)$, so that they are specified just by the central temperature T_c . There is no value of T_c which can account for all the available experimental results. Even if we only consider the Gallium and Kamiokande results, they remain incompatible. Lowering the cross section $p + {}^7\text{Be} \rightarrow \gamma + {}^8\text{B}$ is not a remedy. The shift of the nuclear fusion chain towards the pp -I termination could be induced by a hypothetical low energy resonance in the ${}^3\text{He} + {}^3\text{He}$ reaction. This mechanism gives a somehow better, but still bad fit to the combined experimental data. We also discuss what can be learnt from new generation experiments, planned for the detection of monochromatic solar neutrinos, about the properties of neutrinos and of the Sun.

96.60.Kx

Typeset using REVTeX

I. INTRODUCTION

The aim of this paper is to examine whether there is still room for an astrophysics and/or nuclear physics solution of the solar neutrino problem, in the light of the most recent results of the Gallium experiments [1,2].

We shall demonstrate that these results, when combined with the information arising from the Chlorine [3] and Kamiokande [4] experiments and – most important – with the assumption of a nuclearly powered Sun, severely constrain the individual components of the solar neutrino flux, under the hypothesis of standard (zero mass, no mixing, no magnetic moment . . .) neutrinos.

The arguments leading to these constraints, already outlined in a previous paper [5], are essentially independent of solar models. The basic assumption concerning the Sun is that the *present* total neutrino flux can be derived from the *presently* observed value of the solar constant. We remark that these constraints have become much more stringent after the recent reports from Gallex and Sage [1,2].

For standard neutrinos, these results provide evidence that the nuclear energy production chain, see Fig. 1, is extremely shifted towards the *pp*-I termination and, as a consequence, the fluxes of ν_{Be} and ν_{CNO} are strongly reduced with respect to the predictions of standard solar models.

The situation is the following: i) we can now compare theory and experiment at the level of individual fluxes, ii) the solar neutrino problem, i.e. the discrepancy between experimental results and standard solar models, affects now also the ${}^7\text{Be}$ -nuclei production, and not only the rare ${}^8\text{B}$ neutrinos.

Next, we ask ourselves whether the solar neutrino problem is restricted to standard solar models. In this spirit, we analyze several non-standard solar models with an enhanced *pp*-I termination. The main inputs of any solar model are listed in Table I. We are aware of just two ways for enhancing the *pp*-I termination acting on these inputs:

- i) adjusting the parameters which affect the inner solar temperature, so as to build low inner-temperature solar models,
- ii) adjusting the ${}^3\text{He}$ nuclear cross sections.

We note that the $p + {}^7\text{Be} \rightarrow \gamma + {}^8\text{B}$ cross section does not influence the *pp*-I branch.

As a relevant and common feature of all the low-inner-temperature models, we find a homology relation for the temperature profiles, $T(m) = kT^{\text{SSM}}(m)$, where k depends on the input parameters, but it is independent of the mass coordinate m in the inner radiative zone (at least for $m = M/M_0 < 0.97$), and SSM refers here and in the following to standard solar models. In other words, our numerical experiments disclose that a variation of the solar temperature in the centre implies a definite variation in the entire inner radiative zone.

A consequence of this finding is that the different components of the neutrino flux depend basically only on the central temperature, and are almost independent of how that temperature is achieved. This in turn implies that, when performing a χ^2 analysis of the experimental data compared to the prediction of non-standard solar models, it is sufficient to parameterize these non-standard solar models by the central temperature. In other words, varying independently all the solar model parameters that influence the temperature does not yield a better fit than just varying the central temperature.

It is well known that it is not possible to get a good temperature fit due to the “discrepancy” between the Kamiokande and Chlorine results [6,7], but the following questions are, nonetheless, interesting:

- i) how much does the fit improve if one excludes one of the experimental results?
- ii) does this fit improve if one lowers the $p + {}^7\text{Be} \rightarrow \gamma + {}^8\text{B}$ cross section, as suggested from the analysis of recent data on the Coulomb dissociation of ${}^8\text{B}$ [8,9]?

Another way to shift the nuclear fusion chain towards the pp -I termination without altering the inner solar temperature can be found in the realm of nuclear physics. In the light of the new neutrino results, we discuss whether a hypothetical low energy resonance in the ${}^3\text{He} + {}^3\text{He}$ reaction, firstly advocated by Fowler [10], analyzed in Ref. [6], and presently investigated experimentally at LNGS [11], can reconcile theory and experiments.

Several new-generation experiments are being planned for the detection of monochromatic solar neutrinos produced in electron capture (${}^7\text{Be} + e^- \rightarrow {}^7\text{Li} + \nu$) and in the pep ($p + e^- \rightarrow d + n$) reactions [12–14]. Furthermore, Bahcall [15,16] pointed out that thermal effects on monochromatic neutrino lines can be used to infer inner solar temperatures. In relation with the foregoing analysis, we discuss what can be learnt from such future measurements about the properties of neutrinos and of the Sun.

Concerning the organization of the paper, the solar-model-independent constraints on neutrino fluxes are presented in Sec. II and compared with the results of standard solar models in Sec. III. Section IV is devoted to the analysis of non-standard solar models with lower temperature, which are compared with experimental data in Sec. V. In Sec. VI we discuss the chances of a low energy resonance in the ${}^3\text{He} + {}^3\text{He}$ channel, and in Sec. VII we remark the relevance of future detection of the pep and ${}^7\text{Be}$ neutrinos. Our conclusions are summarized in the final Section.

II. (ALMOST) SOLAR MODEL INDEPENDENT CONSTRAINTS ON NEUTRINO FLUXES

In this section we briefly update the constraints on neutrino fluxes derived in Ref. [5], in the light of the recent reports from Gallex and Sage [1,2]. While we refer to Ref. [5] for details, we recall here the main points.

- i) For standard neutrinos and under the assumption of a nuclearly powered Sun, the components Φ_i of the total neutrino flux arriving onto the Earth are constrained by the equation of energy production

$$K = \sum_i \left(\frac{Q}{2} - \langle E \rangle_i \right) \Phi_i \quad , \quad (1)$$

where K is the solar constant, Q is the energy released in the fusion reaction $4p + 2e \rightarrow \alpha + 2\nu$ and $\langle E \rangle_i$ is the average neutrino energy of the i th flux. In practice the relevant terms in Eq. (1) are just those corresponding to Φ_{pp+pep} , Φ_{Be} , and Φ_{CNO} .

- ii) In order to calculate $\langle E \rangle_i$, we take the ratio $\xi \equiv \Phi_{pep}/\Phi_{pp+pep}$ from the SSM ($\xi = 2.38 \times 10^{-3}$), and, similarly, the ratio $\xi \equiv \Phi_{\text{N}}/\Phi_{\text{CNO}} = 0.54$. Results are almost insensitive to these choices [5].

- iii) The signal S_X of the X experiment is represented as

$$S_X = \sum_i X_i \Phi_i \quad , \quad (2)$$

where the weighting factors X_i are cross sections for the ν detection reaction averaged over the (emission) spectrum of the i -th component of the neutrino flux (note that the X_i are ordered according to the neutrino energy), and are shown in Table II.

iv) We use the following experimental results, where systematic and statistical errors have been added in quadrature. For the Gallium value, we use the weighted average of the Gallex [1] and Sage [2] results

$$S_{\text{Ga}} = (78 \pm 10) \text{ SNU} \quad . \quad (3)$$

For the Chlorine experiment we use the average of the 1970-1992 runs [3]

$$S_{\text{Cl}} = (2.32 \pm 0.26) \text{ SNU} \quad . \quad (4a)$$

Whereas the Kamiokande result reads

$$S_{\text{B}}^{\text{Ka}} = (2.9 \pm 0.42) \times 10^6 \text{ cm}^{-2} \text{ s}^{-1} \quad . \quad (4b)$$

v) We take the Boron flux Φ_{B} , which enters in Eq.(2), from experiment. However, we can use *either* the Kamiokande result *or* the Chlorine result (it is well known [6,7] that a choice between the two experiment is needed, otherwise one is forced to an unphysical value $\Phi_{\text{Be}} \leq 0$).

We have thus four unknowns Φ_{pp+pep} , Φ_{Be} , Φ_{CNO} , and Φ_{B} , which are constrained by the three equations (1), (3), and, alternatively, (4a) or (4b).

By exploiting the ordering properties of the X_i , as discussed in Ref. [5], and by using the new experimental results, one derives severe constraints, for standard neutrinos. As an example, by taking Φ_{B} from Kamioka, for each assumption about Φ_{pp+pep} one has the minimum signal in Gallex if all other neutrinos are from Beryllium and the maximum signal if all other neutrinos are from CNO. By using similar procedures one finds the bounds depicted in Figures. 2, 3, and 4. By conservatively using the Chlorine result to determine the Boron flux (this choice is the less restrictive on the fluxes), we find the following bounds on the fluxes, in units of $10^9 \text{ cm}^{-2} \text{ s}^{-1}$,

$$\begin{aligned} 64 \leq \Phi_{pp+pep} \leq 65 & \quad \text{at } 1 \sigma \\ \Phi_{\text{Be}} & \leq 0.7 \\ \Phi_{\text{CNO}} & \leq 0.6 \quad , \end{aligned} \quad (5a)$$

and

$$\begin{aligned} 61 \leq \Phi_{pp+pep} \leq 65 & \quad \text{at } 3 \sigma \\ \Phi_{\text{Be}} & \leq 4.2 \\ \Phi_{\text{CNO}} & \leq 3.6 \quad . \end{aligned} \quad (5b)$$

In summary, the Gallium result together with the luminosity constraint implies that almost all neutrinos, if standard, come from the pp -I termination. The bounds of Eqs. (5) are very

strict since even a small flux of other (and more energetic) than the pp neutrinos gives an appreciable contribution to the Gallium signal. This is why an experimental result with 10% accuracy can fix the Φ_{pp+pep} at the level of about 2%.

We note that the bounds have become much more stringent than those reported in Ref. [5], because both the central value and the error of the Gallium result have decreased, so that now the experimental result is even closer to the minimal signal which is obtained when all neutrinos come from the pp -I termination ($\Phi_{pp+pep} = 65 \times 10^9 \text{cm}^{-2}\text{s}^{-1}$).

Concerning the assumptions leading to Eqs. (5), we remark that the main hypothesis is that the present Sun is nuclearly powered, see Eq.(1), whereas the values chosen for ξ and η are unessential (see again Ref. [5]).

III. STANDARD SOLAR MODELS AND EXPERIMENTAL DATA

The relevance of the bounds derived in the previous section can be best illustrated by comparing them with the results of standard solar model computations. For a few representative calculations we present the main input parameters of these models in Table III, and the resulting neutrino fluxes in Table IV.

Let us remark that we can now compare not only the total signals predicted by the theory and measured by experiments, but also several individual fluxes, as shown in Table IV. In particular, we find that the upper limit for Φ_{Be} , implied by the experiment at the 1σ level, is 7 times smaller than $\Phi_{\text{Be}}^{\text{SSM}}$, whereas, at the same level of accuracy, the suppression of Φ_{B} is about a factor of two respect to the SSM (in Table IV the experimental upper bound on Φ_{B} is obtained from the less constraining result, i.e. the Kamiokande value). A suppression of Φ_{Be} stronger than Φ_{B} was already implied by the comparison between Kamiokande and Chlorine results, while we derived it using essentially only the Gallium experiments.

In addition, we remind that the theoretical calculation for Φ_{B} is the most questionable of the flux calculations, due to the well known uncertainties. In our opinion, the discrepancy between theory and experiment for the ${}^7\text{Be}$ flux is much more serious than the one for the ${}^8\text{B}$ flux. In other words, it seems to us that the solar neutrino problem is now at the level of the branching between the pp -I and pp -II terminations.

In order to reconcile the theoretical and experimental determination of Φ_{B} , one needs that the ratio between the two rates for the ${}^3\text{He} + {}^4\text{He}$ and the ${}^3\text{He} + {}^3\text{He}$ reactions,

$$R = \frac{\langle \lambda_{34} \rangle}{\langle \lambda_{33} \rangle} \quad , \quad (6)$$

is drastically altered from $R^{\text{SSM}} = 0.16$ to something about $R = 0.02$ (here and in the following, λ_{ij} is the rate for the collision between nuclei with mass number i and j , m_{ij} being the reduced mass).

The investigation of non-standard solar models where R is strongly reduced will be the subject of the next sections. It is worth remarking however that a reduction of Φ_{Be} to bring it in the experimentally acceptable range generally implies also a comparable, or even larger, reduction of Φ_{B} , which then becomes too small with respect to the experimental value.

IV. NON-STANDARD SOLAR MODELS WITH LOW CENTRAL TEMPERATURE

Clearly the pp chain can be shifted towards the pp -I termination by lowering the inner temperature T , since the tunnelling probability is more reduced for the heavier nuclei:

$$\log \left(\frac{\langle \lambda_{34} \rangle}{\langle \lambda_{33} \rangle} \right) \propto \frac{m_{33}^{1/3} - m_{34}^{1/3}}{(KT)^{1/3}} \quad . \quad (7)$$

In order to reduce the inner temperatures one may attempt several manipulations [5]:

- i) reduce the metal fraction Z/X ,
- ii) reduce (by an overall multiplicative factor) the opacity tables,
- iii) increase the astrophysical factor S_{pp} of the $p + p \rightarrow d + e + \nu$ reaction,
- iv) reduce the Sun age.

Clearly i) and ii) work in the direction of getting a more transparent Sun, which implies a lower temperature gradient, a larger energy production region and consequently smaller inner temperatures. When S_{pp} is increased nuclear fusion gets easier, and the fixed luminosity is obtained with a reduced temperature. A younger Sun is another way to get a Sun cooler in its interior, since the central H-abundance is increased and, again, nuclear fusion gets easier.

On the other hand, we remark that variations of the other astrophysical S -factors, S_{33} , S_{34} and/or S_{17} , affect very weakly the inner solar temperature. This is physically clear, since the energy production mechanism is untouched [6].

We have computed several solar models by varying the parameters well beyond the uncertainties of the standard solar model (see Table V), i.e. we have really built non-standard solar models.

An important feature of all these models is the homology of the inner temperature profiles

$$T(m) = kT^{\text{SSM}}(m) \quad , \quad (8)$$

where $m = M/M_0$ is a mass coordinate, and the factor k depends on the parameter which is varied but does not depend on m .

We have verified that Eq. (8) holds with an accuracy better than 1% in all the internal radiative zone ($M/M_0 < 0.97$ or $R/R_0 < 0.7$) for all the models we consider, but for huge (and really unbelievable) variations of the solar age, see Fig. 5 and Table V. It is worth remarking that $T(m)/T^{\text{SSM}}(m)$ is constant through a region where $T(m)$ change by a factor five, see Fig. 6.

By looking at the numerical results, one finds - as expected - that, as long as the Sun age is kept fixed, the models have similar distributions of ^4He and of the energy production per unit mass, which as well known, is strongly related with temperature and ^4He density. On the other hand, when the Sun age is varied, the ^4He content also changes strongly, and the homology relation for the temperature is fading away. The important point is that for each model the temperature profile is essentially specified by a scale factor, which can be taken as the central temperature T_c .

On these grounds one derives general predictions for the behaviour of the neutrino fluxes Φ_i . They are crucially dependent (through the Gamow factors) on the values of the temperature in the production regions T_i , and, as usual, can be locally approximated by power laws:

$$\Phi_i = c_i T_i^{\beta_i} \quad . \quad (9)$$

The homology relationship implies $T_i = (T_c/T_c^{\text{SSM}})T_i^{\text{SSM}}$ and, consequently,

$$\Phi_i = \Phi_i^{\text{SSM}} \left(\frac{T_c}{T_c^{\text{SSM}}} \right)^{\beta_i} \quad . \quad (10)$$

This means that each flux is mainly determined by the central temperature, almost independently on the way the temperature variation was obtained, an occurrence which is clearly confirmed by Fig. 7 for the components of the neutrino flux which give the main contributions (Φ_{pp} , Φ_{Be} , and Φ_{B}) to the experimental signals.

The situation is shown in more details in Table VI where we present the numerically calculated values of the β_i coefficients. One sees that β_{pp} , β_{Be} , and β_{B} are approximately independent on the parameter which is varied. This is not true for Φ_{N} , Φ_{O} , and Φ_{pep} . Actually, when writing Eq. (9) we neglected the flux dependence on the densities of the parent nuclei which generate solar neutrinos. These densities can change when some of the input parameters are varied. For example, Φ_{N} and Φ_{O} look very sensible to variations of Z/X , since in this case, in addition to the temperature variation, the change of metallicity also influences the effectiveness of the CN cycle. However, this effect is negligible when estimating total experimental signals.

Analytical approximations to the numerical values of the β_i can be found by considering the dependence on temperature of the Gamow factors for the relevant nuclear reactions [17]. We would like to comment here just on the temperature dependence of the ratio $\Phi_{\text{B}}/\Phi_{\text{Be}}$:

$$\frac{\Phi_{\text{B}}}{\Phi_{\text{Be}}} = \frac{n_p \langle \sigma_V \rangle_{17}}{n_e \langle \sigma_{V_e} \rangle_{\text{capt}}} \propto \frac{n_p T^{\gamma_{17}}}{n_e T^{\gamma_{\text{capt}}}} \quad , \quad (11)$$

where $\gamma_{\text{capt}} = -1/2$, and $\gamma_{17} = -2/3 + E_{17}/KT$ (E_{17} is the Gamow peak for the $p + {}^7\text{Be} \rightarrow \gamma + {}^8\text{B}$ reaction) [18]. Assuming n_p/n_e to be constant, and evaluating E_{17}/KT at T_c^{SSM} , we get

$$\frac{\Phi_{\text{B}}}{\Phi_{\text{Be}}} \propto T_c^{13.5} \quad . \quad (12)$$

This value is in good agreement with the one reported in Table VI for a S_{pp} variation; the agreement is less good with the values obtained by varying the other parameters (in this case n_p/n_e is clearly not conserved).

Therefore, as long as the temperature profile is *unchanged*, lowering the temperature immediately implies that Boron neutrinos are suppressed much more strongly than Beryllium neutrinos, since the penetrability factor for the $p + {}^7\text{Be} \rightarrow \gamma + {}^8\text{B}$ reaction is diminished.

V. THE CENTRAL SOLAR TEMPERATURE AND THE EXPERIMENTAL RESULTS.

From the argument just presented, it is clear that a central temperature reduction cannot work; nevertheless, let us perform a $\chi^2(T_c)$ analysis to see quantitatively what happens. We define:

$$\chi^2(T_c) = \sum_{XY} (S_X^{\text{ex}} - S_X^{\text{th}}) V_{XY}^{-1} (S_Y^{\text{ex}} - S_Y^{\text{th}}) \quad , \quad (13)$$

where the symbols have the following meaning.

- i) The experimental signals S_X^{ex} ($X = \text{Gallium, Chlorine and Kamiokande}$) are the ones reported in Eqs. (3) and (4).
- ii) The theoretical signals $S_X^{\text{th}}(T_c)$ are calculated according to the formula

$$S_X^{\text{th}} = \sum_{i \neq pp} X_i \Phi_i^{\text{SSM}} \left(\frac{T_c}{T_c^{\text{SSM}}} \right)^{\beta_i} + X_{pp} \Phi_i^{pp} \quad , \quad (14)$$

where we take the β coefficients corresponding to the S_{pp} variations (second column of Table VI), and we use the CDF94 standard solar model results, see Table IV. Note, in particular, that Φ_B^{SSM} has been calculated by using $S_{17} = 22.4$ eV barn. In order to achieve a better accuracy, Φ_{pp} is calculated directly through the Eq. (1).

iii) The error matrix V_{XY} takes into account both the experimental and the theoretical uncertainties. The theoretical uncertainties are due to the neutrino cross sections X_i , and to the solar model parameters that are not related to the free parameter T_c , i.e. S_{33} , S_{34} , and S_{17} . The diagonal entries, V_{XX} , are the sum of the experimental variance σ_X^2 , plus the squares of the errors due to the cross sections $\sum_i (\Delta_X^i)^2$ (Δ_X^i is the error of the detection cross section for the X experiment averaged over the i -th flux), plus the squares of the errors due to the input parameters S_{33} , S_{34} , and S_{17} , i.e. $\sum_P (\Delta_X^P)^2$ ($P = S_{33}, S_{34}, S_{17}$). The off-diagonal entries have contributions only from these last errors: $V_{XY} = \sum_P \Delta_X^P \Delta_Y^P$. The errors Δ are calculated by linear propagation. Therefore, if we call δ_X^i the error on the cross section X_i , $\Delta_X^i = \Phi_i^{\text{SSM}} \left(\frac{T_c}{T_c^{\text{SSM}}} \right)^{\beta_i} \delta_X^i$, while, if δ^P is the error on the parameter P , $\Delta_X^P = \left(\partial S_X^{\text{th}} / \partial P \right) \delta^P$. The partial derivative of the neutrino fluxes respect to these parameters are estimated by using power-laws which we have been determined from numerical experiments, and which are very similar to those of Table 7.2 in Ref. [19]. The values we use for the uncertainties of the SSM parameters, δ^P , are given in Table I, while the errors on the cross sections, δ_X^i , can be found in Table II. The use of the error matrix is necessary to avoid that an apparently good fit be achieved in an unphysical way, e.g. we cannot use the uncertainty of the Boron flux to strongly reduce its contribution to the Davis experiment, and, at the same time, have a smaller reduction in the Kamiokande experiment.

The results shown in Fig. 8(a) deserve a few comments.

- i) The best fit to the three experimental signals yields a $\chi_{\text{min}}^2[\text{Cl+Ga+Ka}] = 18.5$ that, for two degrees of freedom, is excluded at the 99.99% level (here we have treated systematic and statistical errors on equal footing); we thus confirm the results of Ref. [20]. This is partly due to the well known ‘‘inconsistency’’ between Kamiokande and Chlorine.
- ii) Even if we only consider Gallium and Kamiokande the fit is still poor, yielding a $\chi_{\text{min}}^2[\text{Ga+Ka}] = 11$, that for one degree of freedom is excluded at the 99.9% level. The reason is that if one tries to reduce Φ_{Be} in accordance with Gallium data, then Φ_{B} becomes too small in comparison with the Kamiokande result. On the other hand, if one considers just Gallium and Chlorine results the situation is better ($\chi_{\text{min}}^2[\text{Cl+Ga}] = 5$, which has a 2.5% probability), due to the fact that the smaller Boron (and Beryllium) signal implied by the Chlorine experiment can be more easily adjusted to the Gallium result.

iii) From the above discussion it is clear that if one lowers the $p + {}^7\text{Be} \rightarrow \gamma + {}^8\text{B}$ cross section, the situation gets even worse, see Fig. 8(b). In other words, a reduction of S17 does not solve the solar neutrino problem.

iv) Considering the Chlorine data corresponding (approximately) to the same data taking period as the other experiments ($S_{\text{Cl}}^{88-92} = 2.76 \pm 0.31$ SNU [3]) the situation is only slightly changed: $\chi_{\text{min}}^2[\text{Cl}+\text{Ga}+\text{Ka}] = 15$ that, for two degrees of freedom, is excluded at the 99.94% level; $\chi_{\text{min}}^2[\text{Ga}+\text{Ka}] = 11$, that for one degree of freedom is excluded at the 99.9% level; and $\chi_{\text{min}}^2[\text{Cl}+\text{Ga}] = 6$, which has a 2.4% probability.

v) For the uncertainties of Table I, the effect of the error correlation is not large: for instance, if we use uncorrelated errors $\chi_{\text{min}}^2[\text{Cl}+\text{Ga}+\text{Ka}] = 16$ instead of 18.5. The real importance of error correlation becomes evident if we try to resolve the discrepancy by increasing the errors. For example, doubling the uncertainties reduces the uncorrelated χ_{min}^2 to 14, while the correlated one practically does not change.

vi) The situation does not significantly change when considering models where one of the other parameters (opacity table, Z/X, age) are varied instead of S_{pp} , as it is shown by Fig. 9. Slightly better fits are obtained by varying Z/X or the age than S_{pp} or the opacities, but the resulting $\chi_{\text{min}}^2[\text{Cl}+\text{Ga}+\text{Ka}] = 16.5$ is still excluded at the 99.97% level.

vii) If one insists on a low temperature solution, the best fit is for $T_c/T_c^{\text{SSM}} \approx 0.94$, i.e. $T_c = 1.46 \times 10^7 \text{ }^\circ\text{K}$. The price to pay for this 6% temperature reduction is very high in terms of the input parameters which are being varied, see Table I. Huge variations of the parameters are required, and, furthermore, in many cases the values used are at the border of what can be tolerated by our stellar evolution code: for example, we are not able to produce a Sun with $T_c/T_c^{\text{SSM}} < 0.94$ by lowering the opacity or the age.

VI. A LOW ENERGY RESONANCE IN THE ${}^3\text{HE} + {}^3\text{HE}$ CHANNEL?

As mentioned in the introduction, the other way to enhance the pp -I termination is to play with the ${}^3\text{He}$ nuclear cross sections. As it was shown in Ref. [6], if the astrophysical S-factors are varied by a constant (through the star) quantity:

$$\Phi_i = \Phi_i^{\text{SSM}} \theta \quad (15a)$$

where

$$\theta = \frac{S_{34}}{S_{34}^{\text{SSM}}} \sqrt{\frac{S_{33}^{\text{SSM}}}{S_{33}}} \quad \text{and} \quad i = \text{B, Be} \quad . \quad (15b)$$

Numerical experiments confirm the approximate validity of Eqs. (15) giving $\Phi_{\text{B,Be}} = \Phi_{\text{B,Be}}^{\text{SSM}} \theta^{0.9}$. Note that the changes of Φ_{B} and Φ_{Be} are proportional.

For variations of S_{33} and S_{34} the solar temperature is essentially unaffected, and, consequently, all the fluxes other than B and Be are also unaffected. Only the $pp + pep$ neutrino flux slightly changes, in order to fulfill the luminosity condition, Eq. (1), i.e.

$$\Phi_{pp+pep} = \Phi_{pp+pep}^{\text{SSM}} + \Phi_{\text{Be}}^{\text{SSM}} - \Phi_{\text{Be}} \quad (16)$$

In order to reduce the Beryllium flux by a factor – say – three with respect to the SSM value, S_{33} (S_{34}) has to be nine times (one third) the value used in the standard solar model

calculations. Clearly, what matters are the values of the astrophysical factors at the energies relevant in the Sun, i.e. at the position of the Gamow peak for the He + He reactions near the solar center, $E_G \approx 20$ keV.

We recall that the astrophysical factors used in the calculations are obtained by extrapolating experimental data taken at higher energies (see Ref. [18] for a review). Thus a very low energy resonance in the ${}^3\text{He} + {}^3\text{He}$ reactions could be effective in reducing Φ_{Be} and Φ_{B} , and could have escaped to experimental detection. This possibility, first advanced in Ref. [10], cannot be completely dismissed, (see the discussion in Refs. [6,18]) and it is presently being investigated in the underground nuclear physics experiment LUNA at Laboratori Nazionali del Gran Sasso [11].

For a resonance at energy E_r and with strength $\omega\gamma$, equations (15) become:

$$\Phi_i = \Phi_i^{\text{SSM}} \sqrt{\frac{1}{1+x_i}} \quad i = \text{B, Be} \quad , \quad (17a)$$

where

$$x_i = \frac{\omega\gamma}{W} \exp[3A(KT_i)^{-1/3} - E_r/(KT_i)] \quad , \quad (17b)$$

and T_i are the temperatures at the peak of the ν_{Be} and ν_{B} production ($T_{\text{Be}} = 1.45 \times 10^7$ °K, $T_{\text{B}} = 1.5 \times 10^7$ °K), K is the Boltzmann constant, and the other constants, defined in Ref. [6], are $W = 20.4$ keV and $A = 1.804$ MeV $^{1/3}$.

Let us remark that the resonance can work differently in different regions of the Sun, in relationship with the kinetic energies of the colliding particles. A low energy resonance is more efficient in the outer zone of energy production, and consequently Φ_{Be} can be suppressed more than Φ_{B} . The opposite occurs for higher energy resonances, the turning point being $E_r \approx E_G$, see Ref. [6] for details.

We have performed a χ^2 analysis as a function of the resonance strength $\omega\gamma$ for several values of the resonance energy E_r , with a procedure quite similar to that used in the previous section.

The errors on the calculated signals arise from the neutrino interaction cross sections, from S_{17} , and from all those quantities which influence the estimated central temperature of the Sun (S_{pp} , Z/X , opacity and age), but not from S_{33} and S_{34} that influence fluxes according to Eq. (15), and correspond to our free parameter. Again, the derivative of the neutrino fluxes with respect to these parameters, necessary to calculate the error matrix by linear propagation, are estimated by using power-laws very similar to those of Table 7.2 in Ref. [19].

The uncertainties we use are shown in Tables I and II. We note that uncertainties on the absorption cross sections, the metallicity Z/X and the opacity are the most important for estimating the errors on the signal. For the opacity we followed Ref. [21] and took “the characteristic difference between the solar interior opacity calculated with Livermore and with Los Alamos opacity code”, which may or may not be a fair estimate of the uncertainty, but we could not find a better prescription. However, as we shall see, the correlation among the errors is such that χ_{min}^2 does not change even if we double the uncertainties on Z/X and on the opacity.

The results are presented in Fig. 10. The situation looks slightly better than in the low temperature models since the Φ_{Be} reduction does not imply an even stronger Φ_{B} reduction. However, the best $\chi_{\text{min}}^2 = 14$, obtained for $E_r = 0$, is still excluded at the 99.9% level. The χ_{min}^2 slightly increases with E_r because of the tuning of the Beryllium/Boron suppression.

The best fit strength as a function of E_r is shown in Fig. 11, together with existing experimental upper bound. We expect that LUNA experiment, presently performed at LNGS [11], will have a sensitivity better by about a factor 100, as compared with previous experiments, mainly due to the cosmic ray shielding in the underground laboratory, so that the search should be able to detect/exclude such a resonance down to extremely low values of E_r .

The use of the properly correlated errors on the fluxes is even more important when studying the effect of the hypothetical resonance than when we changed the temperature. The χ_{min}^2 would be 10 instead of 14, had we used uncorrelated errors. Moreover, doubling the errors would yield a χ_{min}^2 of almost 6, while the correlated one remains 14. The intuitive explanation of how the uncorrelated fit works is the following. The Chlorine and Kamiokande results require different suppressions of the neutrino fluxes. The fit finds the best compromise between the two experiments by adjusting the resonance strength. Then, the uncertainty on the temperature is used to further deplete Φ_{Be} and, at the same time, to increase Φ_{B} , which is clearly unphysical. The correlated fit correctly uses the uncertainty on the temperature either to increase or to decrease both fluxes at the same time: either option is useless, once we get the best compromise for the common reduction of the two fluxes, no matter how much we are allowed to change the temperature.

Combining the two mechanisms, i.e. a resonance in a low temperature model, does not work either, since again, once the best compromise suppression of the ${}^7\text{Be}$ and ${}^8\text{B}$ fluxes is achieved by one of the two mechanisms, the other cannot do much more.

VII. THE DETECTION OF *pep* AND ${}^7\text{Be}$ NEUTRINOS

New generation experiments are being planned for the detection of monochromatic solar neutrinos produced in electron capture (${}^7\text{Be} + e^- \rightarrow {}^7\text{Li} + \nu$) and in the *pep* ($p + e^- + p \rightarrow d + \nu$) reactions [12–14]. Furthermore, Bahcall [15,16] pointed out that, from the measurement of the average energy difference between neutrinos emitted in solar and laboratory decay, one can infer the temperature of the production zone. In this section we discuss what can be learnt from such future measurements about the properties of neutrinos and of the Sun.

Concerning the intensity of the ${}^7\text{Be}$ line, we recall the bounds of Eqs. (5): at 1σ (3σ) the neutrino flux has to be smaller than $0.7 \times 10^9 \text{cm}^{-2}\text{s}^{-1}$ ($4.0 \times 10^9 \text{cm}^{-2}\text{s}^{-1}$), otherwise neutrinos are non-standard. We recall however that a low Φ_{Be} is also typical of the MSW solution, see Fig. 12.

The *pep* neutrinos are a good indicator of Φ_{pp} , since the ratio Φ_{pep}/Φ_{pp} is rather stable. In Fig. 12 we see that standard neutrinos correspond to Φ_{pep} in the range $(1 \div 2) \times 10^8 \text{cm}^{-2}\text{s}^{-1}$, whereas the MSW solution requires $\Phi_{pep} \leq 3 \times 10^7 \text{cm}^{-2}\text{s}^{-1}$. Thus, a measurement of the *pep*-line intensity will be crucial for deciding about neutrino properties.

The possibility of measuring inner solar temperatures through thermal effects on monochromatic neutrino lines looks to us extremely fascinating (although remote). In this

respect the homology relationship, Eq. (8), is particularly interesting, see Fig. 13.

If homology holds, a measurement of the solar temperature in the – say – ${}^7\text{Be}$ production zone gives the value of T_c . On the other hand, the homology relation itself is testable – in principle – by comparing the temperatures at two different places, as can be done by looking at the shapes of both the ν_{Be} and ν_{pep} lines. We remark that this would be a test of the mechanism for energy transport through the inner Sun.

VIII. CONCLUSIONS

i) If neutrinos are standard, the present solar neutrino experiments already impose severe constraints on the individual components of the total neutrino flux. These constraints, at the 1σ level, are:

$$\begin{aligned}\Phi_{\text{Be}} &\leq 0.7 \times 10^9 \text{cm}^{-2}\text{s}^{-1} \\ \Phi_{\text{CNO}} &\leq 0.6 \times 10^9 \text{cm}^{-2}\text{s}^{-1} \\ 64 \times 10^9 \text{cm}^{-2}\text{s}^{-1} &\leq \Phi_{\text{pep}} \leq 65 \times 10^9 \text{cm}^{-2}\text{s}^{-1}\end{aligned}\tag{18}$$

The constraint on Beryllium neutrinos is in strong disagreement with the results of any standard solar model calculation, see Table IV. The solar neutrino problem is now at the Beryllium production level: the experimental data demand a strong shift towards the pp -I termination, and the problem is not restricted anymore to the rare pp -III (${}^8\text{B}$) termination.

ii) Solar models with low inner temperatures show temperature profiles $T(m)$ homologous to that of the Standard Solar Model: $T(m) = kT^{\text{SSM}}(m)$. As a consequence, the main components of the neutrino flux depend essentially on the central solar temperature T_c (see Table V), and the experimental signals can be parameterized in terms of T_c . As already known, there is no value of T_c which can account for all the available experimental results ($\chi_{\text{min}}^2(T_c) \approx 16$). In addition, we find that the fit is poor even considering just Gallium and Kamiokande results ($\chi_{\text{min}}^2(T_c) \approx 11$). Furthermore, lowering the cross section for $p + {}^7\text{Be} \rightarrow \gamma + {}^8\text{B}$ makes things worse.

iii) Alternatively, the shift of the nuclear fusion chain towards the pp -I termination could be induced by a hypothetical low energy resonance in the ${}^3\text{He} + {}^3\text{He}$ reaction. This mechanism gives a somehow better but still poor fit to the combined experimental data ($\chi_{\text{min}}^2(T_c) \approx 14$). Its possible relevance to the solar neutrino problem will be elucidated in an underground nuclear physics experiment, presently performed at LNGS.

iv) Concerning future experiments, the measurement of the ${}^7\text{Be}$ and, particularly, of the pep -line intensities will be crucial for discriminating non-standard solar models from non-standard neutrinos, in relation with the bounds in Eq (18). Furthermore, the homology relation itself can be tested, in principle, in experiments aimed at the measurement of inner solar temperatures by looking at thermal effects on the pep and Be line shapes. This would provide a clear test about the mechanism of energy transport in the solar interior.

In conclusion, we feel that recent Gallium results, taken at their face value, strongly point towards non-standard neutrinos. Of course we are anxiously waiting for the calibration of Gallex and Sage, and for future experiments.

ACKNOWLEDGMENTS

One of us (G. F.) acknowledges useful discussions with V. Berezhinsky.

REFERENCES

- [1] GALLEX Collaboration, P. Anselman *et al.*, Report No. LNGS-94/89 (1993), to be published in Phys. Lett. B
- [2] V. N. Gavrin, in talk given at 6th International Symposium on Neutrino Telescopes, Venice, Italy, February 1993.
- [3] R. Davis Jr., Proc. of the 23rd ICRC, Calgary, Canada (1993), Prog. in Nucl. and Part. Phys. **32** (1994).
- [4] A. Suzuki, "Kamiokande results and prospects", talk given at 6th International Symposium on Neutrino Telescopes, February 1993, Venice.
- [5] V. Castellani *et al.*, Phys. Lett. B **324**, 245 (1994).
- [6] V. Castellani, S. Degl'Innocenti and G. Fiorentini, A.& A. **271**, 601 (1993).
- [7] S. A. Bludman *et al.*, Phys. Rev. D **45**, 1810 (1992).
- [8] K. Langanke and T. D. Shoppa, Phys. Rev C **49**, 1771 (1994).
- [9] T. Motobayashi *et al.*, Rikkyo Report No. RUP-94/2, 1994, submitted to Phys. Rev. Lett.
- [10] W. A. Fowler, Nature **238**, 24 (1972).
- [11] C. Arpesella *et al.*, Nuclear Astrophysics at Gran Sasso Laboratory (Proposal for a pilot project with a 30 KeV accelerator) internal report LNGS 91-18 (1991).
- [12] C. Arpesella *et al.*, Borexino at Gran Sasso: Proposal for a Real-Time Detector for Low Energy Solar Neutrinos, internal report INFN - Milan (1992).
- [13] A. Alessandrello *et al.*, Report No. INFN/AE-92/28 (1992).
- [14] R. S. Raghavan *et al.*, Report No. AT&T Bell Laboratories Technical Memorandum 11121-930824-27TM (1993).
- [15] J. N. Bahcall, Phys. Rev Lett. **71**, 2369 (1993).
- [16] J. N. Bahcall, Report No. IASSNS-AST 93/40 (1994), to be published in Phys. Rev. D.
- [17] V. Castellani, S. Degl'Innocenti and G. Fiorentini, Phys. Lett B **303**, 68 (1993).
- [18] C. Rolfs and W. Rodney, *Cauldrons in the Cosmos* (Chicago University Press, Chicago, USA, 1988).
- [19] J. N. Bahcall, *Neutrino Astrophysics* (Cambridge University Press, Cambridge, England, 1989).
- [20] S. A. Bludman *et al.*, Phys. Rev. D **47**, 2220 (1993).
- [21] J. N. Bahcall and M. H. Pinsonneault, Rev. Mod. Phys. **60**, 297 (1992).
- [22] J. N. Bahcall and M. Kamionkowski, Astrophys. J. **420**, 884 (1994).
- [23] S. Turck-Chièze *et al.*, Phys. Rep. **230**, 57 (1993).
- [24] A. Garcia *et al.*, Phys. Rev. Lett. **67**, 3654 (1991).
- [25] S. Turck-Chièze and I. Lopez, Astrophys. J. **408**, 347 (1993).
- [26] R. Iglesias and Wilson, Astrophys. J. **397**, 717 (1992).
- [27] N. Grevesse, in proceedings of Evolution of Stars: the Photospheric Abundance connection, IAU, 1991, eds. G. Michaud and A. Tutukov.
- [28] C. W. Johnson *et al.*, Astrophys. J. **392**, 320 (1992).
- [29] A. Krauss *et al.*, Nucl. Phys. A **467**, 273 (1987).
- [30] G. Fiorentini *et al.*, Report No. INFNFE-10/93 (1993), to appear in Phys. Rev. D (1994).

TABLES

TABLE I. The main parameters P of solar models and their estimated relative uncertainties at 1σ level, $(\delta^P/P)^{\text{SSM}}$ (here as in the text $\delta^P \equiv \delta P$). All values are as in Ref. [21], apart for S_{pp} , which is taken from the more recent Ref. [22]. Concerning solar age we refer to common wisdom, see Ref. [23]. In the last column we show, for the first four parameters, the values of $\zeta \equiv P/P^{\text{SSM}}$ needed to account for $T_c/T_c^{\text{SSM}} = 0.94$, when each input parameter is varied separately. In the same column we also show, for S_{33} and S_{34} , the values needed to account for $\Phi_{\text{Be}} = 0.3 \Phi_{\text{Be}}^{\text{SSM}}$ (again when each input parameter is varied separately).

P	$\left(\frac{\delta^P}{P}\right)^{\text{SSM}}$	$\zeta = \frac{P}{P^{\text{SSM}}}$
S_{pp}	1%	1.7
opacity	2.5%	0.63
Z/X	6%	0.30
age	3%	0.23
S_{33}	6%	11.0
S_{34}	3%	0.3
S_{17}	9%	–

TABLE II. For the i -th component of the neutrino flux we show the average neutrino energy $\langle E \rangle$ and the averaged neutrino capture cross sections X_i ($1 \text{ SNU cm}^2 \text{ s} = 10^{-36} \text{ cm}^2$) for Chlorine (Cl) and Gallium (Ga), with errors at 1σ level. All data are from Ref. [19], but for the Cl cross section average over the ${}^8\text{B}$ neutrino flux, which is taken from Ref. [24]. When averaging the pp and pep components we use the relative weights of our SSM (CDF94), see Table III; similarly for ${}^{13}\text{N}$ and ${}^{15}\text{O}$.

	$\langle E \rangle$ [MeV]	Cl [$10^{-9}\text{SNU cm}^2\text{s}$]	Ga [$10^{-9}\text{SNU cm}^2\text{s}$]
pp	0.265	0.	1.18(1 ± 0.02)
pep	1.442	1.6 (1 ± 0.02)	21.5 (1 ± 0.07)
$pp + pep$	0.268		1.23(1 ± 0.02)
${}^7\text{Be}$	0.814	0.24(1 ± 0.02)	7.32(1 ± 0.03)
${}^{13}\text{N}$	0.707	0.17(1 ± 0.02)	6.18(1 ± 0.03)
${}^{15}\text{O}$	0.996	0.68(1 ± 0.02)	11.6 (1 ± 0.06)
CNO (${}^{13}\text{N} + {}^{15}\text{O}$)	0.840	0.40(1 ± 0.02)	8.67(1 ± 0.05)
${}^8\text{B}$	6.71	1090. (1 ± 0.01)	2430. (1 ± 0.25)

TABLE III. Physical input parameters of several Standard Solar Models. We show the solar mass $M_0[10^{33}\text{gr}]$, the solar radius $R_0[10^{10}\text{cm}]$, the solar luminosity $L_0[10^{33}\text{erg/s}]$, the solar age $[10^9\text{yr}]$, the metal to hydrogen mass fraction Z/X , the zero energy astrophysical S -factors $[MeV\text{ barn}]$ and their derivatives with respect to energies S' $[\text{barn}]$. BP is “the best model with diffusion” of Ref. [21]; TCL is the “IS Cpp Recent CNO model” of Ref. [25]; CDF94 is our updated standard solar model, with Livermore opacity table [26], chemical composition following Grevesse 1991 “low iron” [27], and without diffusion.

physical quantities	BP	TCL	CDF94
M_0	1.989	1.989	1.989
R_0	6.96	6.96	6.96
L_0	3.86	3.85	3.83
Age	4.6	4.5	4.6
Z/X	2.67×10^{-2}	2.43×10^{-2}	2.67×10^{-2}
$S(0)_{pp}$	4.00×10^{-25}	4.00×10^{-25}	3.89×10^{-25}
$S'(0)_{pp}$	4.52×10^{-24}	4.67×10^{-24}	4.52×10^{-24}
$S(0)_{33}$	5.00	5.00	5.00
$S'(0)_{33}$	-0.9	-0.9	-0.9
$S(0)_{34}$	5.33×10^{-4}	5.4×10^{-4}	5.33×10^{-4}
$S'(0)_{34}$	-3.1×10^{-4}	-3.10×10^{-4}	-3.10×10^{-4}
$S(0)_{17}$	2.24×10^{-5}	2.24×10^{-5}	2.24×10^{-5}
$S'(0)_{17}$	-3.00×10^{-5}	-3.00×10^{-5}	-3.00×10^{-5}
$S(0)_{12C+p}$	1.45×10^{-3}	1.40×10^{-3}	1.40×10^{-3}
$S'(0)_{12C+p}$	2.45×10^{-3}	4.24×10^{-3}	4.24×10^{-3}
$S(0)_{13C+p}$	5.50×10^{-3}	5.50×10^{-3}	5.77×10^{-3}
$S'(0)_{13C+p}$	1.34×10^{-2}	1.34×10^{-2}	1.40×10^{-2}
$S(0)_{14N+p}$	3.32×10^{-3}	3.20×10^{-3}	3.32×10^{-3}
$S'(0)_{14N+p}$	-5.91×10^{-3}	-5.71×10^{-3}	-5.91×10^{-3}
$S(0)_{15N(p,\gamma)16O}$	6.40×10^{-2}	6.40×10^{-2}	6.40×10^{-2}
$S'(0)_{15N(p,\gamma)16O}$	3.00×10^{-2}	3.00×10^{-2}	3.00×10^{-2}
$S(0)_{15N(p,\alpha)12C}$	7.80×10	5.34×10	7.04×10
$S'(0)_{15N(p,\alpha)12C}$	3.51×10^2	–	4.21×10^2
$S(0)_{16O+p}$	9.40×10^{-3}	9.40×10^{-3}	9.40×10^{-3}
$S'(0)_{16O+p}$	-2.30×10^{-2}	-2.30×10^{-2}	-2.30×10^{-2}

TABLE IV. Comparison among recent Standard Solar Model predictions and experimental results. For the definition of BP, TCL and CDF94 see Table III. We show the central temperature T_c [10^7 °K], the Helium abundance in mass Y, the metallicity fraction Z, the values of each component of the neutrino flux [10^9 cm $^{-2}$ s $^{-1}$], the calculated signals for the Chlorine (Cl) and the Gallium (Ga) experiments [SNU]. On the right side we present the experimental constraints at one and three standard deviation level.

	Standard Solar Models			Experimental Constraints		
	BP	TCL	CDF94	1σ	3σ	from
T_c	1.569	1.543	1.564			
Y	0.273	0.271	0.289			
Z ($\times 10^2$)	1.96	1.88	1.84			
pp	60.0	60.4	60.0			
pep	0.14	0.14	0.14			
$pp + pep$	60.14	60.54	60.14	≥ 64.0	≥ 61.0	Ga + Cl
${}^7\text{Be}$	4.89	4.25	4.79	≤ 0.70	≤ 4.23	Ga + Cl
${}^8\text{B}$ ($\times 10^3$)	5.69	4.14	5.6	≤ 3.30	≤ 4.10	Ka
${}^{13}\text{N}$	0.49	0.36	0.47			
${}^{15}\text{O}$	0.43	0.30	0.40			
${}^{13}\text{N} + {}^{15}\text{O}$	0.92	0.66	0.87	≤ 0.6	≤ 3.6	Ga + Cl
${}^{17}\text{F}$ ($\times 10^3$)	5.4	–	4.8			
hep ($\times 10^6$)	1.2	–	1.3			
Cl	8.0	6.1	7.8	≤ 2.6	≤ 3.0	Cl
Ga	132	121	130	≤ 88	≤ 108	Ga

TABLE V. Test of the homology relationships. We show $k = \langle T(m)/T(m)^{\text{SSM}} \rangle$, and its r.m.s. variation Δk for several non-standard models, obtained by varying: $s_{pp} = S_{pp}/S_{pp}^{\text{SSM}}$, opa = opacity / opacity^{SSM}, $z = (Z/X)/(Z/X)^{\text{SSM}}$, and $t = \text{age} / \text{age}^{\text{SSM}}$. The averages are performed over the mass shells in the region **(a)** $M/M_0 \leq 0.3$, and **(b)** $M/M_0 \leq 0.97$.

(a)											
S_{pp} variation			opacity variation			Z/X variation			age variation		
s_{pp}	k	Δk [10 ⁻³]	opa	k	Δk [10 ⁻³]	z	k	Δk [10 ⁻³]	t	k	Δk [10 ⁻³]
1.25	0.976	1.36	0.9	0.988	0.72	0.5	0.962	1.46	0.9	0.996	2.16
1.5	0.955	2.58	0.7	0.958	2.71	0.3	0.939	2.17	0.7	0.987	6.56
1.75	0.939	3.04	0.6	0.939	3.71	0.2	0.925	2.40	0.4	0.979	10.6
2.0	0.925	3.58				0.1	0.904	4.20	0.2	0.971	14.8
2.5	0.902	4.45							0.1	0.966	17.3
3.5	0.868	5.43									
(b)											
S_{pp} variation			opacity variation			Z/X variation			age variation		
s_{pp}	k	Δk [10 ⁻³]	opa	k	Δk [10 ⁻³]	z	k	Δk [10 ⁻³]	t	k	Δk [10 ⁻³]
1.25	0.977	1.82	0.9	0.989	1.07	0.5	0.962	2.80	0.9	1.00	4.17
1.5	0.957	1.88	0.7	0.962	4.00	0.3	0.938	4.48	0.7	1.00	12.8
1.75	0.941	5.00	0.6	0.944	5.17	0.2	0.923	5.98	0.4	0.999	21.0
2.0	0.928	6.48				0.1	0.902	8.45	0.2	1.00	2.97
2.5	0.905	10.3							0.1	1.00	14.8
3.5	0.870	17.4									

TABLE VI. The β_i coefficients of the power laws that describe the dependence of the neutrino fluxes on the temperature ($\Phi_i = \Phi_i^{\text{SSM}}(T_c/T_c^{\text{SSM}})^{\beta_i}$). The components of neutrino flux that we consider are shown in the first column. The values presented are the best fit to the numerical calculations performed when each input parameter is varied in the range specified in the first row (same notation as Table IV).

	s_{pp} 1 ÷ 3.5	opa 0.6 ÷ 1	z 0.1 ÷ 1	t 0.1 ÷ 1
pp	-0.60	-0.63	-0.73	-0.85
${}^7\text{Be}$	8.74	9.51	10.8	11.4
${}^{15}\text{N}$	15.1	12.0	30.9	8.58
${}^{16}\text{O}$	23.51	15.7	35.6	17.6
pep	2.20	-2.23	-1.71	0.49
${}^8\text{B}$	22.3	20.76	21.5	20.2

FIGURES

FIG. 1. The pp chain.

FIG. 2. The Gallium signal S_{Ga} is shown as a function of the neutrino flux Φ_{pp+pep} . Standard neutrinos correspond to the area inside the full (dot-dashed) lines if the Kamiokande (Chlorine) value for the Boron contribution is used. The Gallium result $\pm 1\sigma$ is shown. The lower limit for the pp -I flux is thus $\Phi_{pp+pep}^{\text{min}} = 64.2 \times 10^9 \text{cm}^{-2}\text{s}^{-1}$ ($64.6 \times 10^9 \text{cm}^{-2}\text{s}^{-1}$) The upper limit $\Phi_{pp+pep}^{\text{max}} = 64.8 \times 10^9 \text{cm}^{-2}\text{s}^{-1}$ is given by the luminosity constraint.

FIG. 3. The Gallium signal S_{Ga} is shown as a function of the neutrino flux Φ_{Be} . The Gallium result $\pm 1\sigma$ is shown (dashed lines). For standard neutrinos, the allowed region is above the straight line $S_{\text{Ga}}^{\text{min}}$. The region consistent with the Gallium result and standard neutrinos is the shaded area. The allowed flux has to be smaller than $\Phi_{\text{Be}} = 7 \times 10^8 \text{cm}^{-2}\text{s}^{-1}$ ($4 \times 10^8 \text{cm}^{-2}\text{s}^{-1}$), at 1σ , if the Boron contribution is derived from Chlorine (Kamiokande) experiment. The result of our SSM is also shown (\diamond).

FIG. 4. The Gallium signal S_{Ga} is shown as a function of the neutrino flux Φ_{CNO} . The Gallium result $\pm 1\sigma$ is shown (dashed lines). For standard neutrinos, the allowed region is above the straight line $S_{\text{Ga}}^{\text{min}}$. The region consistent with the Gallium result and standard neutrinos is the shaded area. The allowed flux has to be smaller than $\Phi_{\text{CNO}} = 6 \times 10^8 \text{cm}^{-2}\text{s}^{-1}$ ($2 \times 10^8 \text{cm}^{-2}\text{s}^{-1}$), at 1σ , if the Boron contribution is derived from Chlorine (Kamiokande) experiment. The result of our SSM is also shown (\diamond).

FIG. 5. The temperature profiles $T(m)$ normalized to $T^{\text{SSM}}(m)$ for a few representative non-standard solar models.

FIG. 6. The SSM temperature profile $T^{\text{SSM}}(m)$, normalized to the central value T_c^{SSM} .

FIG. 7. The behaviour of Φ_{pp} , Φ_{Be} , and Φ_{B} as a function of the central temperature T_c when varying S_{pp} , opacity, Z/X and age.

FIG. 8. The χ^2 as a function of the central temperature T_c . (a) We use the standard value $S_{17} = 22.4 \text{ eV barn}$ [28]. (b) We use the recently proposed value $S_{17} = 12 \text{ eV barn}$ [8].

FIG. 9. The χ^2 as a function of the central temperature T_c when the temperature variation is obtained by changing the different input parameters.

FIG. 10. For a few values of the resonance energy E_r , we show χ^2 as a function of the resonance strength $\omega\gamma$. The fit is done with all (Ga+Cl+Ka) data.

FIG. 11. The best fit strength $\omega\gamma$ of the ${}^3\text{He} + {}^3\text{He}$ resonances as a function of the resonance energy E_r (full line). The arrows correspond to the experimental upper bounds on the resonance strength, from Ref. [29].

FIG. 12. The pep neutrino flux (Φ_{pep}) vs. the ${}^7\text{Be}$ neutrino flux (Φ_{Be}). For the standard solar model (\diamond). For several non-standard solar models adjusted so as to reproduce the Gallium result within 3σ (the Boron contribution is taken from the Kamiokande experiment); the notation is as in Fig. 7, and the number close to each point represents the corresponding value of $\zeta = P/P^{\text{SSM}}$. The values for the MSW solution, corresponding to the best fit (\times), and to the 90% C.L. region (dots), see also Ref. [30].

FIG. 13. Relations among the temperatures T_i at the ${}^7\text{Be}$ and pep peak production zones ($R/R_0 = 0.06$ and $R/R_0 = 0.09$, respectively), and the central temperature T_c in non-standard solar models. Data from numerical calculations are shown with the same symbols as in Fig. 7, while full lines show the homology relations $T_i = T_c (T_i^{\text{SSM}}/T_c^{\text{SSM}})$.

This figure "fig1-1.png" is available in "png" format from:

<http://arxiv.org/ps/astro-ph/9405064v1>

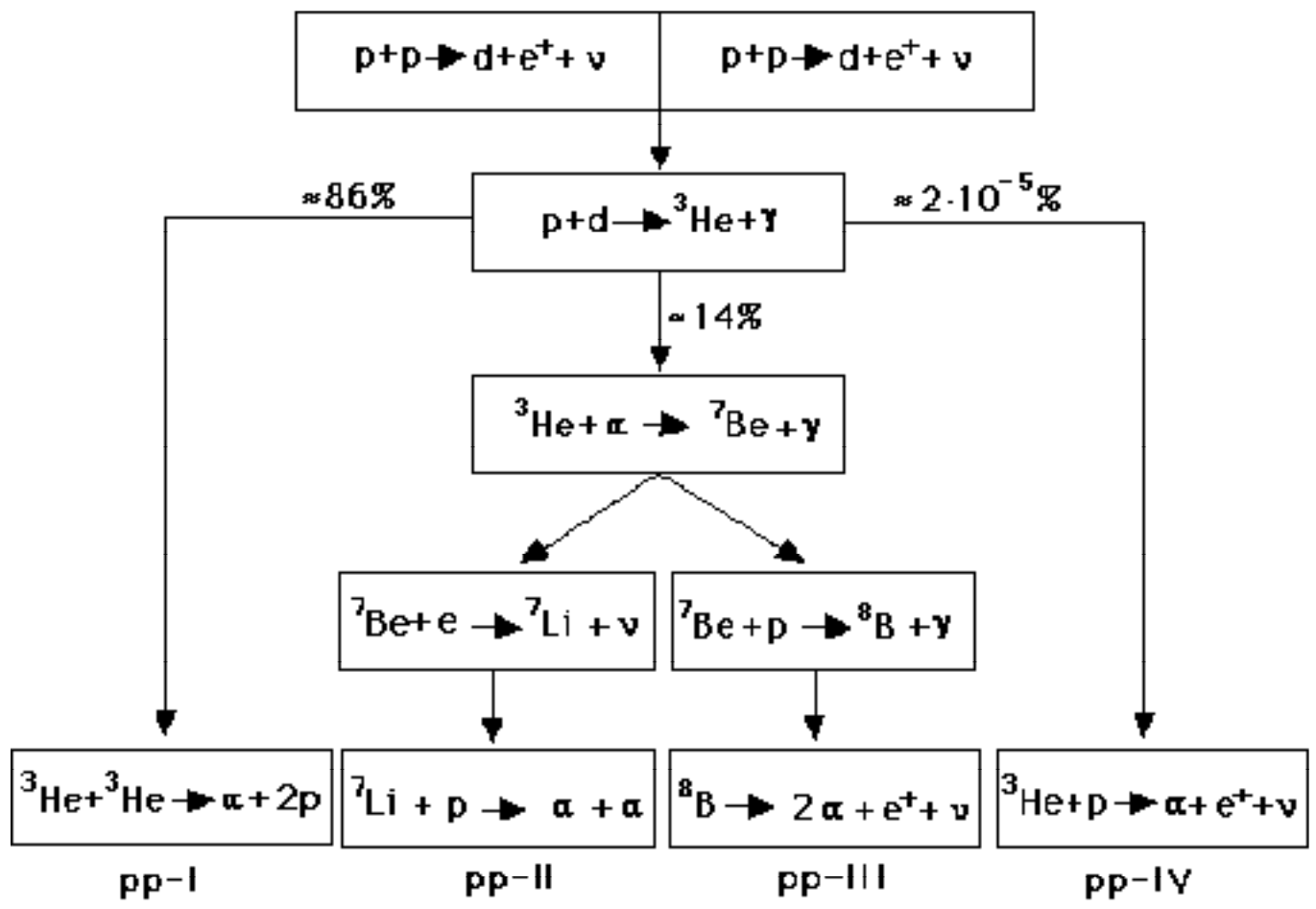


Fig. 1

This figure "fig2-1.png" is available in "png" format from:

<http://arxiv.org/ps/astro-ph/9405064v1>

This figure "fig3-1.png" is available in "png" format from:

<http://arxiv.org/ps/astro-ph/9405064v1>

This figure "fig4-1.png" is available in "png" format from:

<http://arxiv.org/ps/astro-ph/9405064v1>

This figure "fig2-2.png" is available in "png" format from:

<http://arxiv.org/ps/astro-ph/9405064v1>

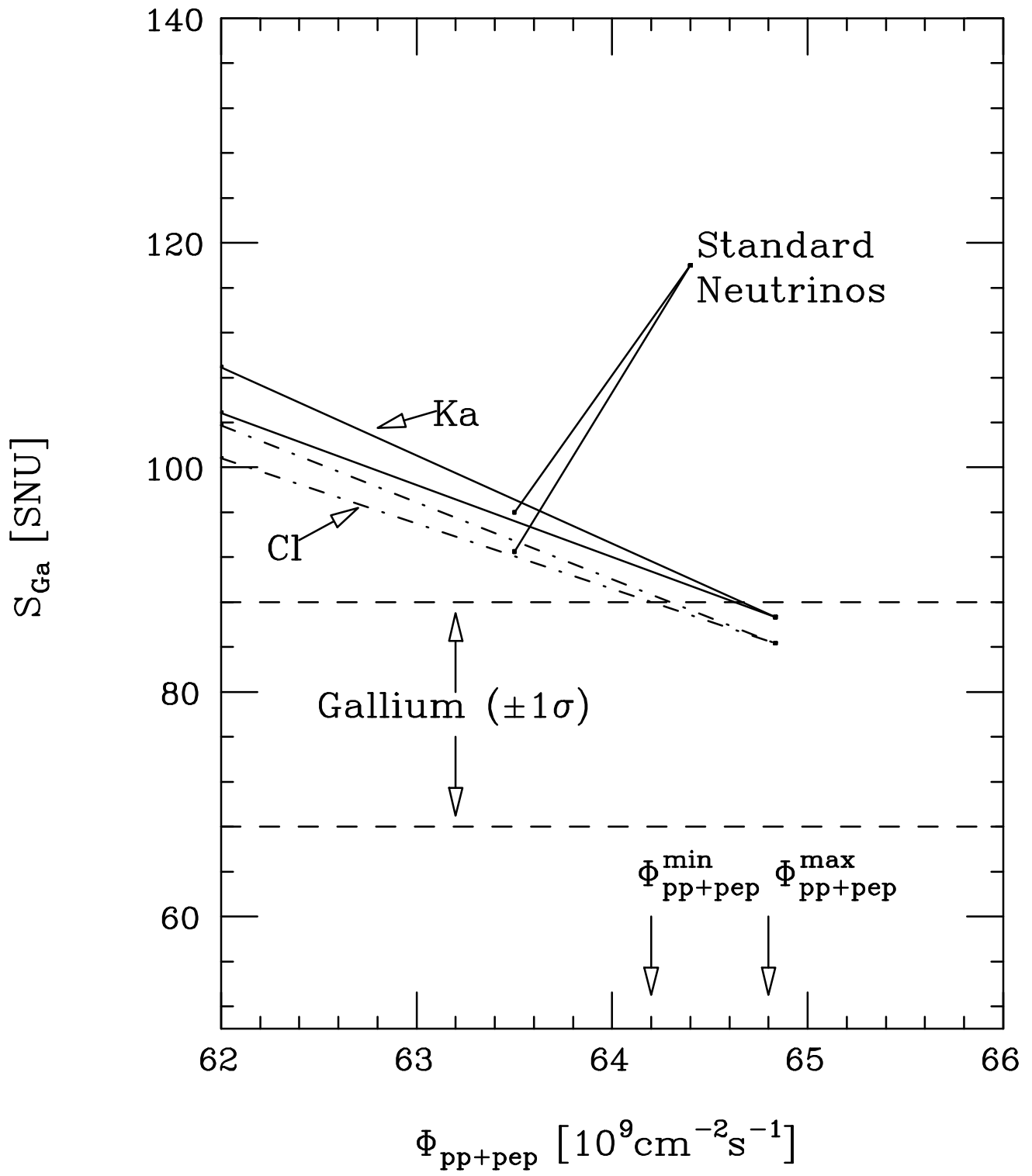


Fig. 2

This figure "fig3-2.png" is available in "png" format from:

<http://arxiv.org/ps/astro-ph/9405064v1>

This figure "fig4-2.png" is available in "png" format from:

<http://arxiv.org/ps/astro-ph/9405064v1>

This figure "fig2-3.png" is available in "png" format from:

<http://arxiv.org/ps/astro-ph/9405064v1>

This figure "fig3-3.png" is available in "png" format from:

<http://arxiv.org/ps/astro-ph/9405064v1>

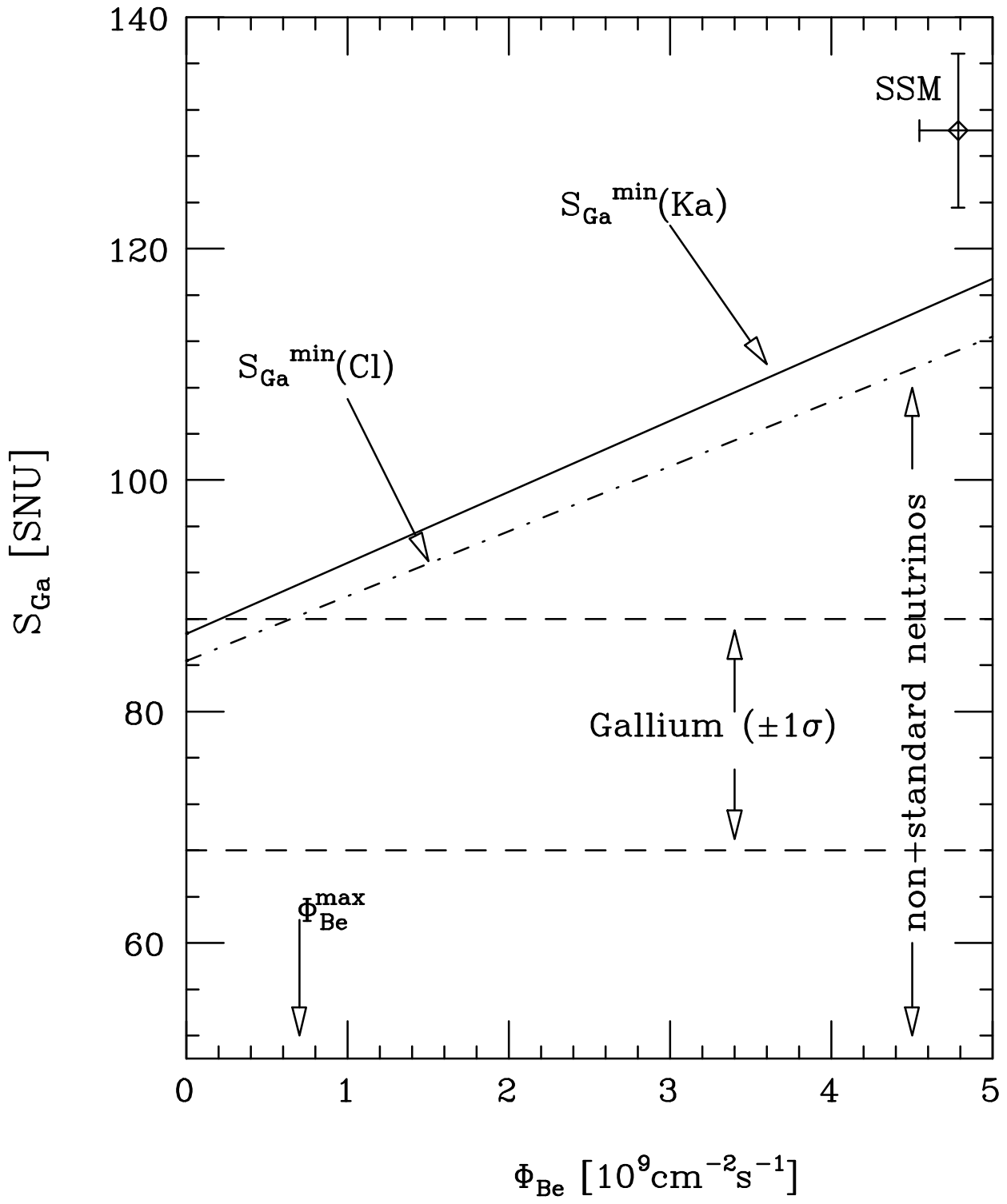


Fig. 3

This figure "fig4-3.png" is available in "png" format from:

<http://arxiv.org/ps/astro-ph/9405064v1>

This figure "fig2-4.png" is available in "png" format from:

<http://arxiv.org/ps/astro-ph/9405064v1>

This figure "fig3-4.png" is available in "png" format from:

<http://arxiv.org/ps/astro-ph/9405064v1>

This figure "fig4-4.png" is available in "png" format from:

<http://arxiv.org/ps/astro-ph/9405064v1>

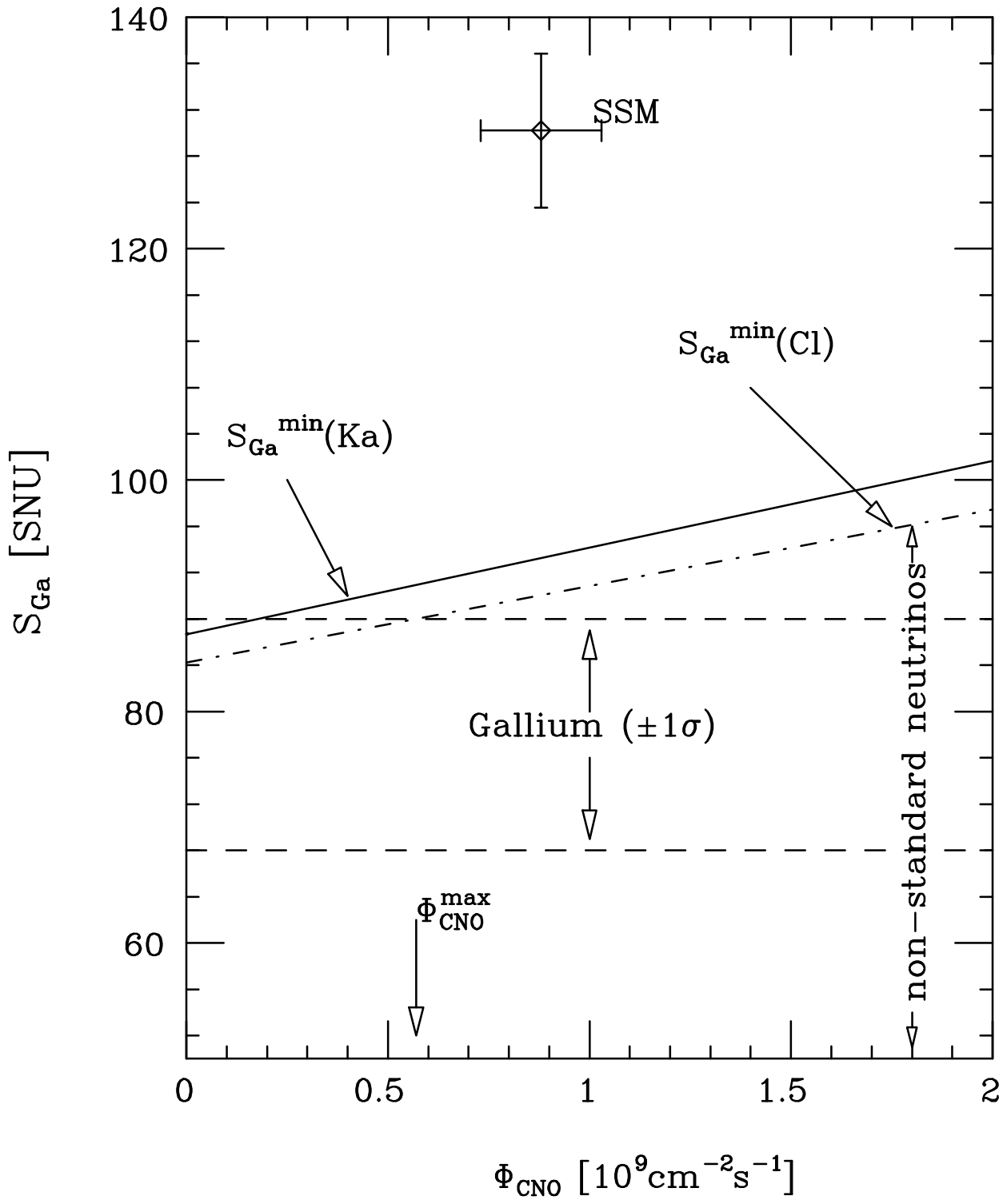


Fig. 4

This figure "fig3-5.png" is available in "png" format from:

<http://arxiv.org/ps/astro-ph/9405064v1>

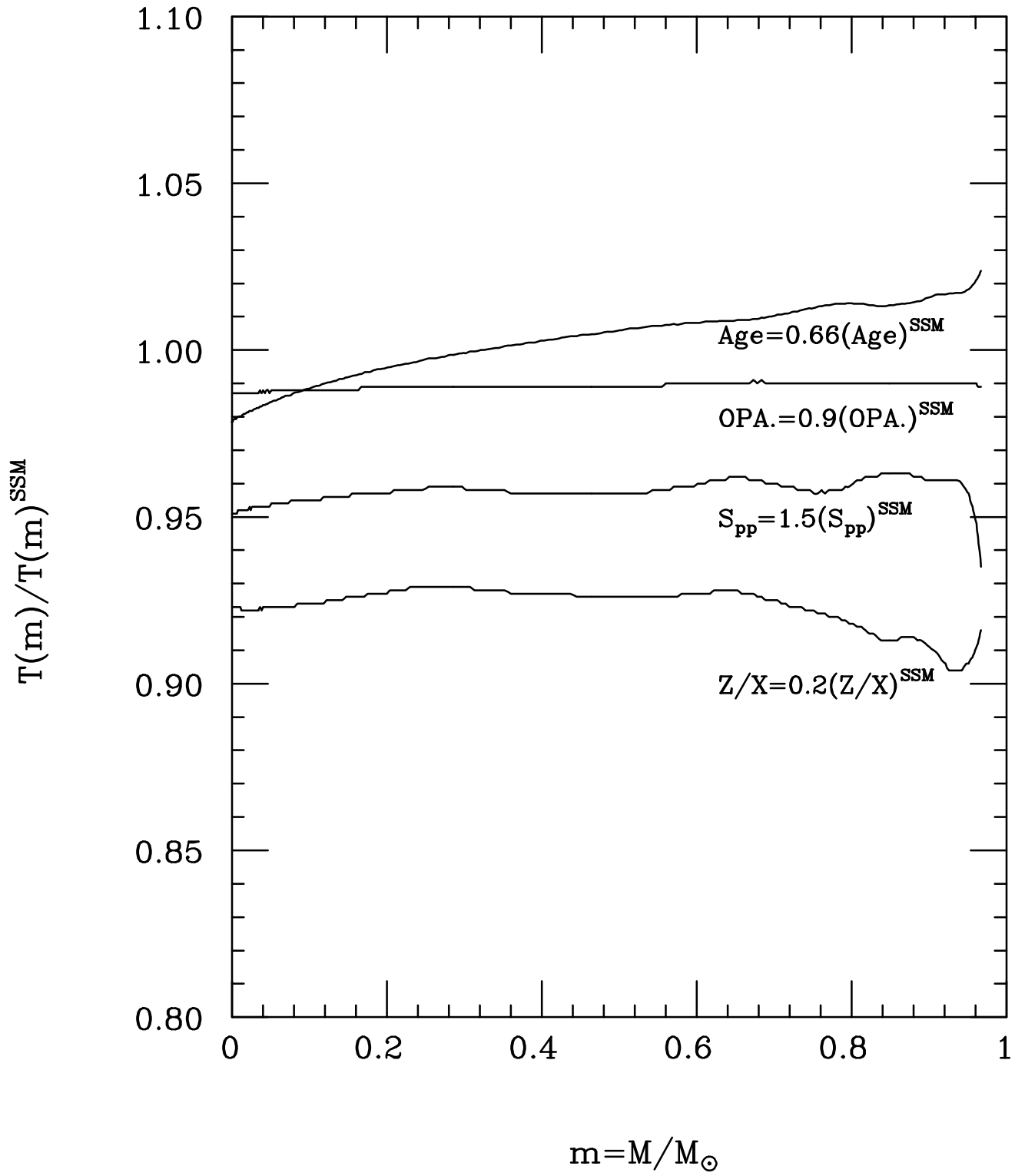


Fig. 5

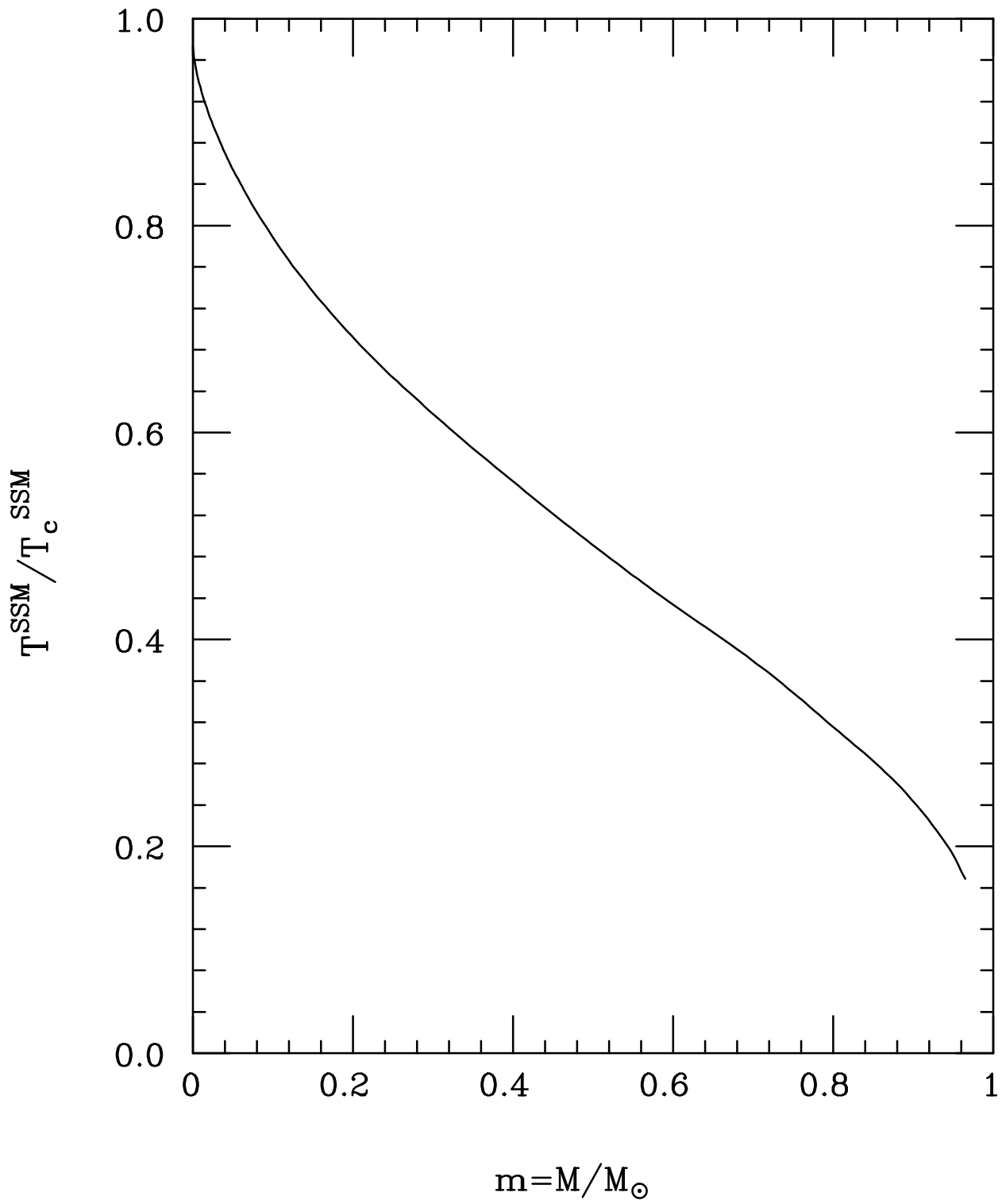


Fig. 6

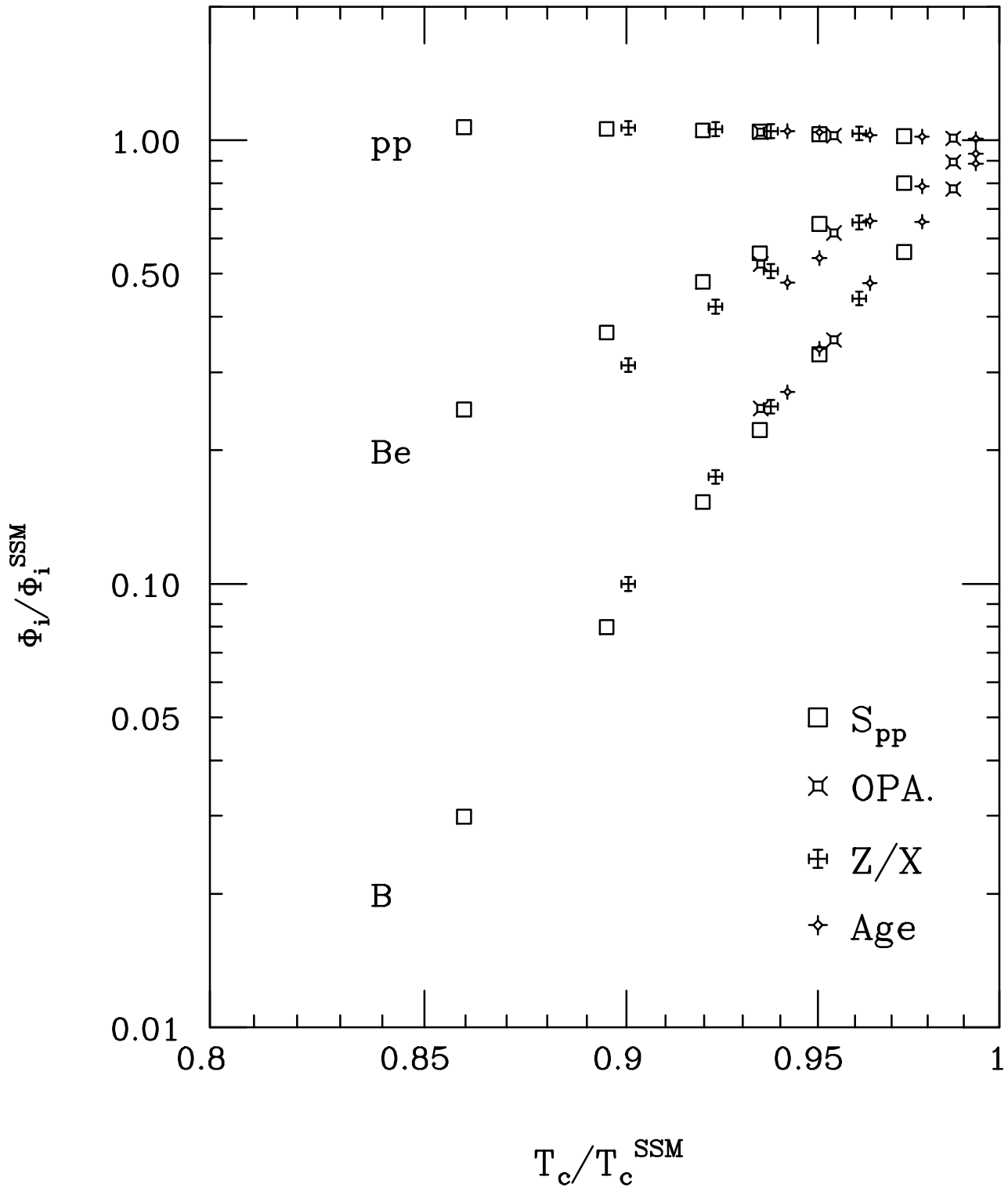


Fig. 7

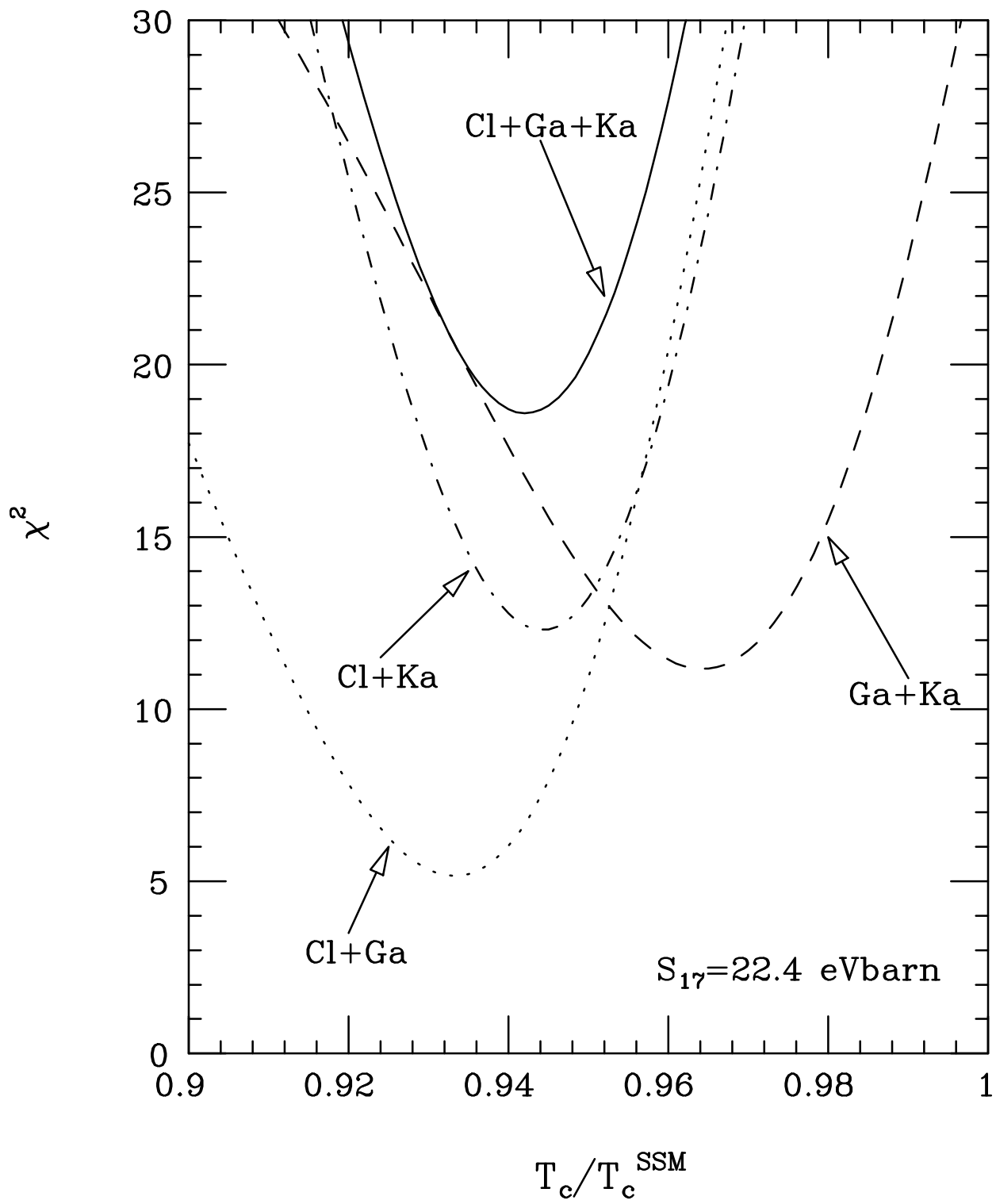


Fig. 8a

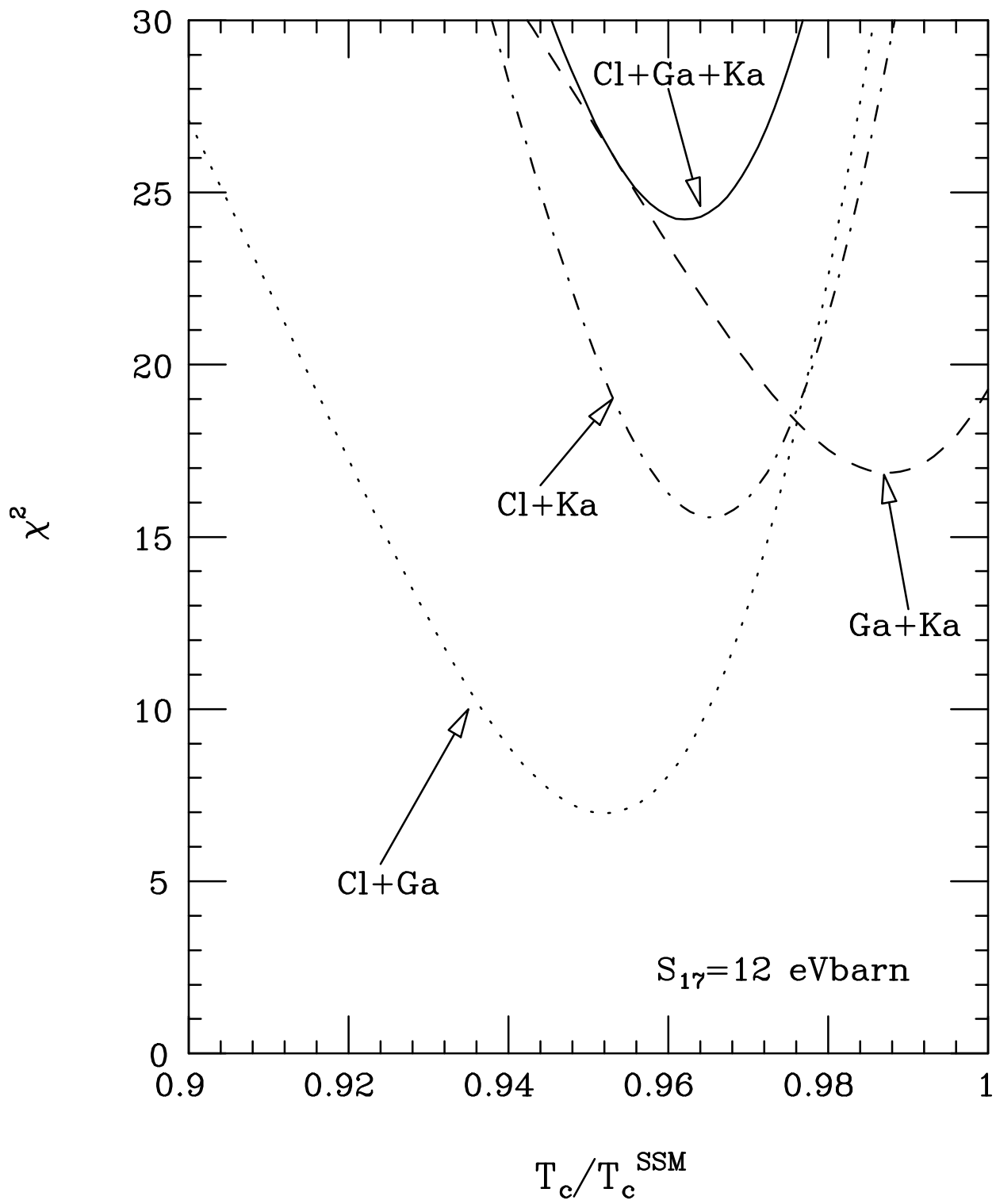


Fig. 8b

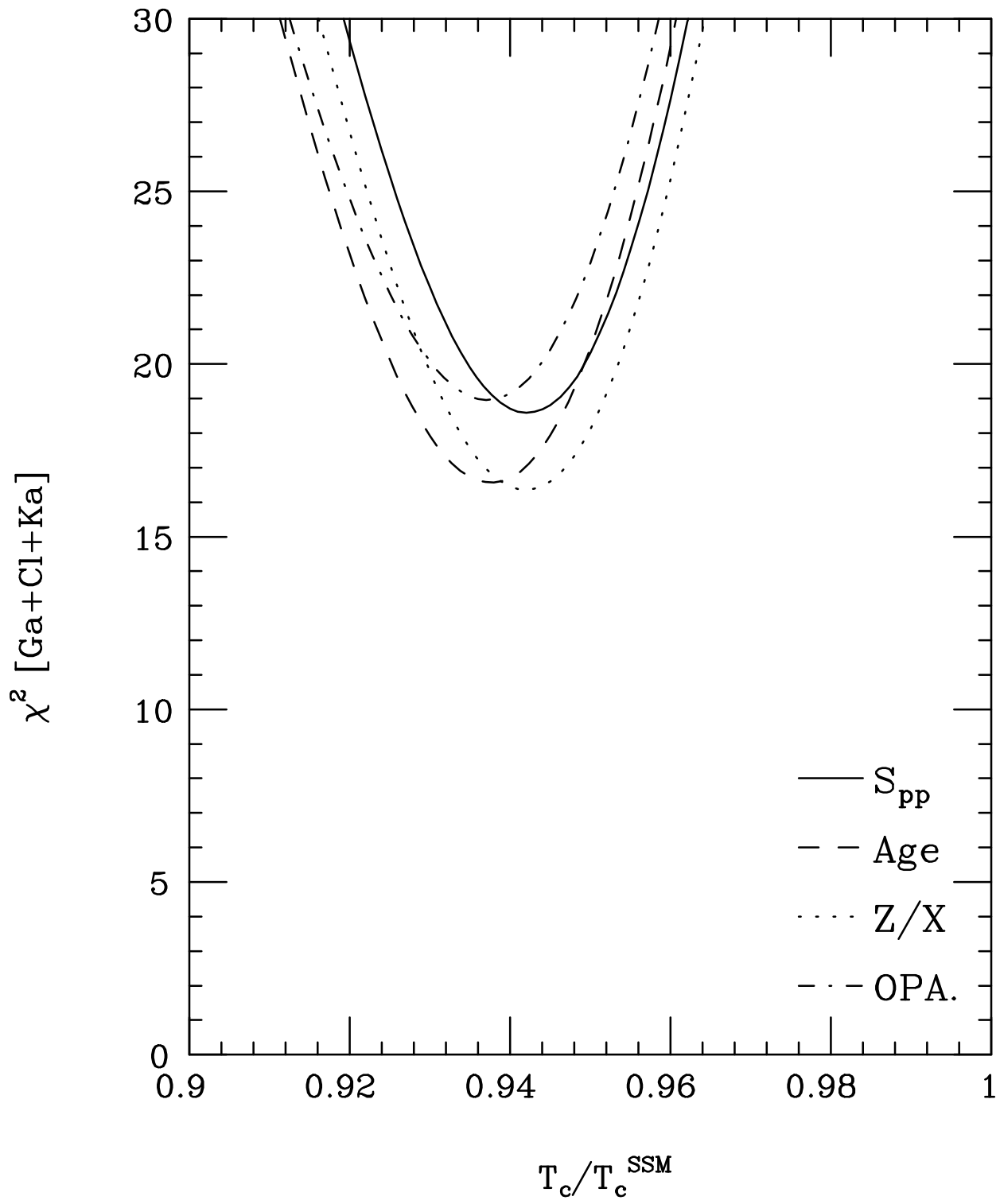


Fig. 9

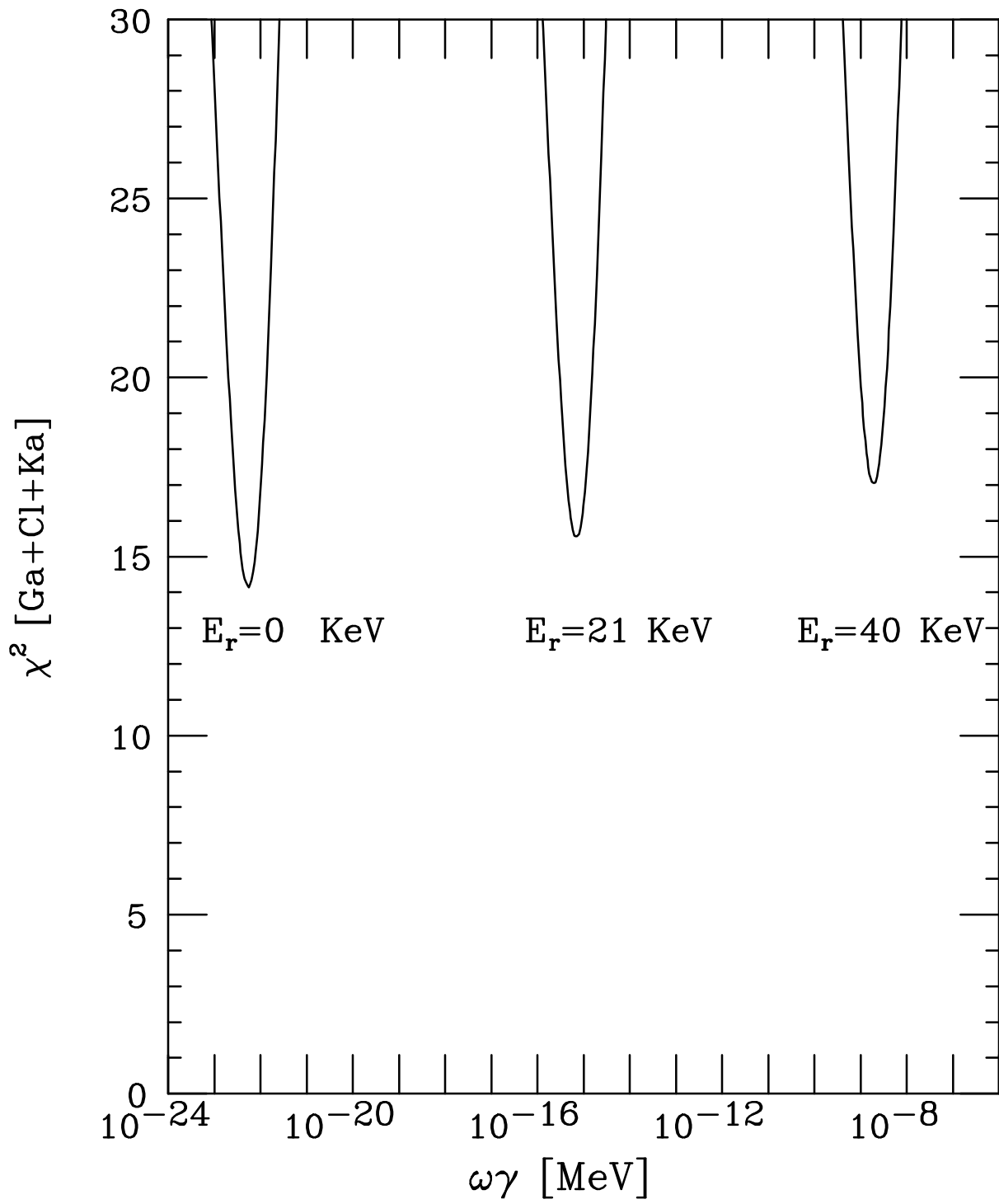


Fig.10

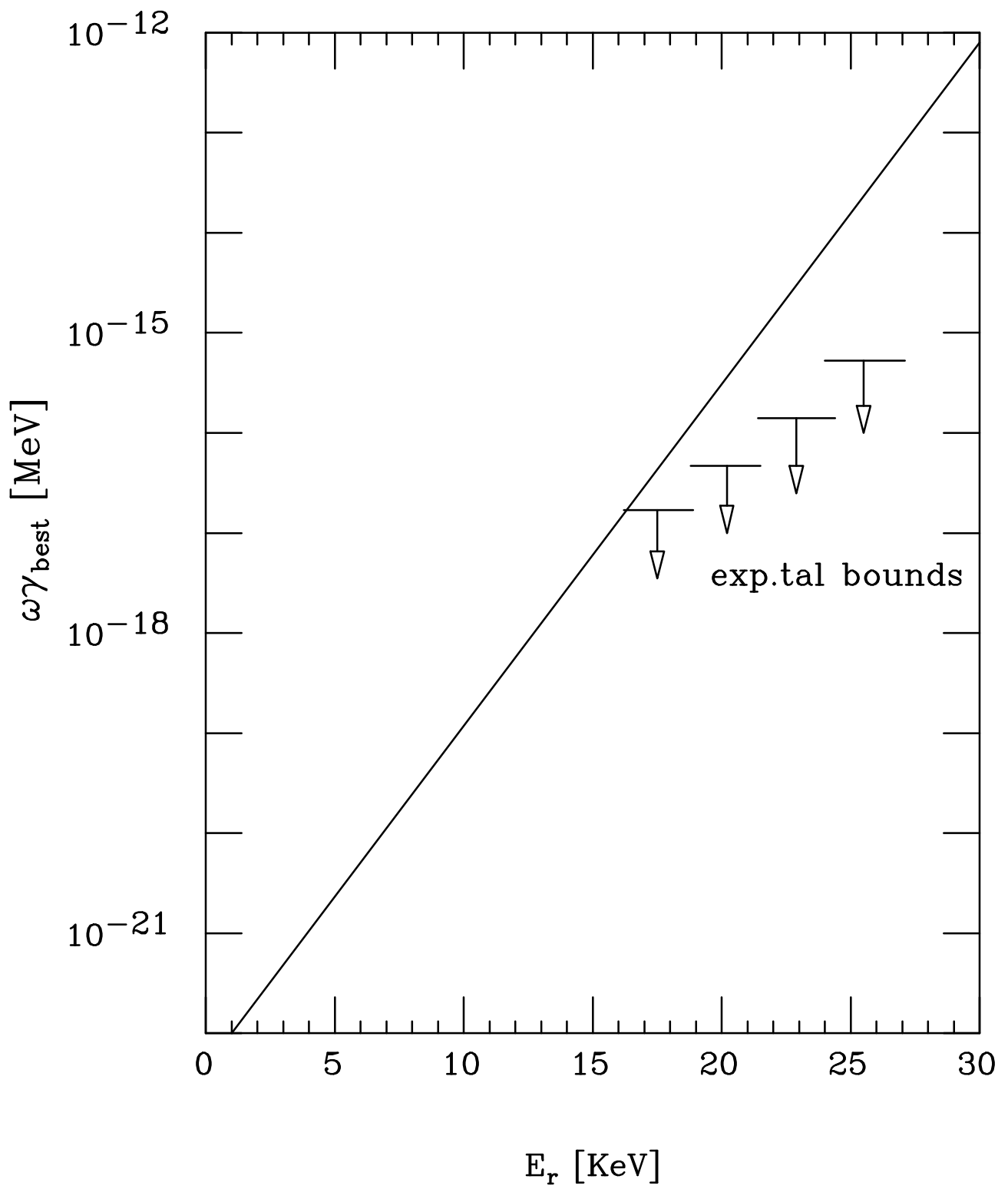


Fig. 11

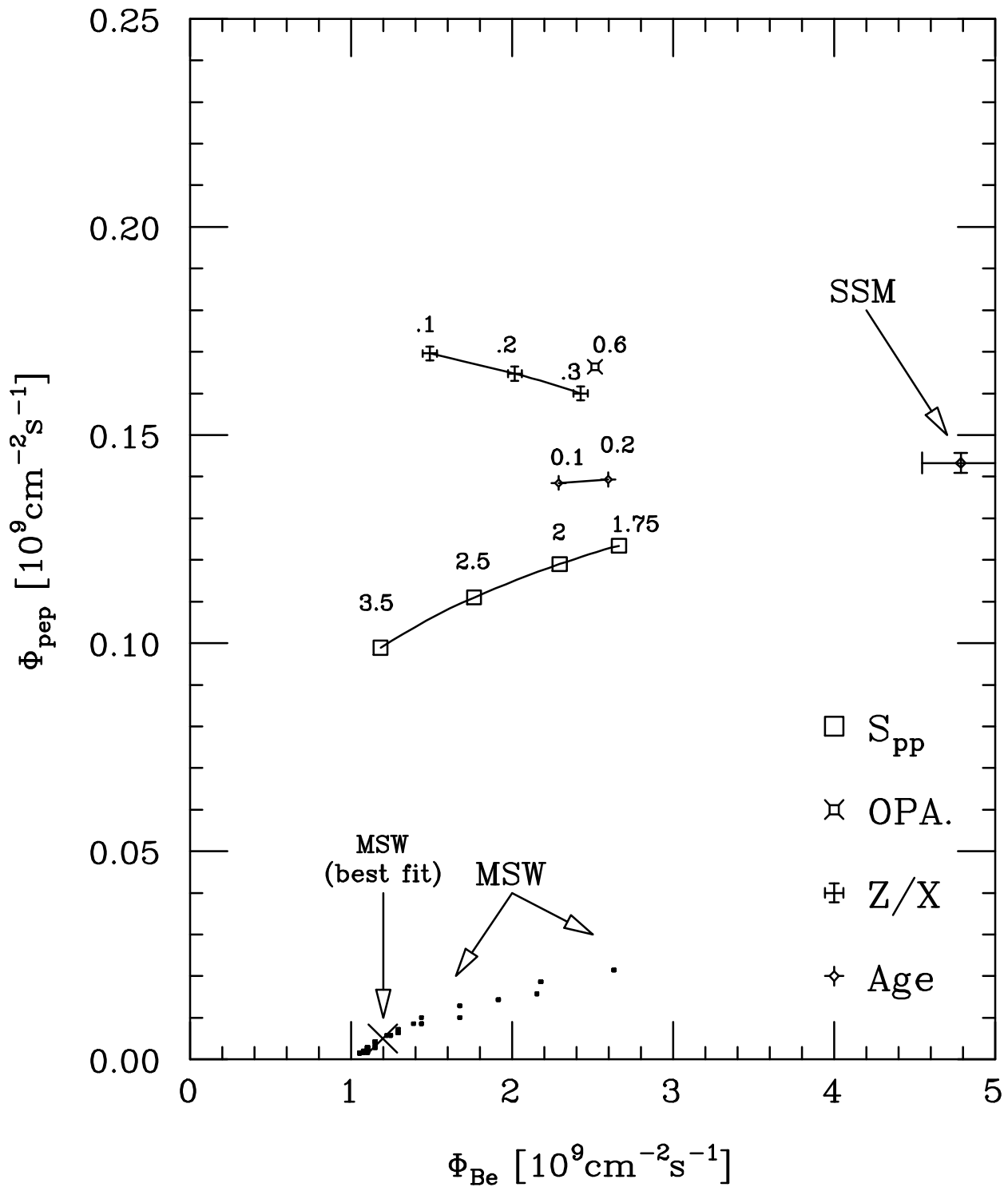


Fig. 12

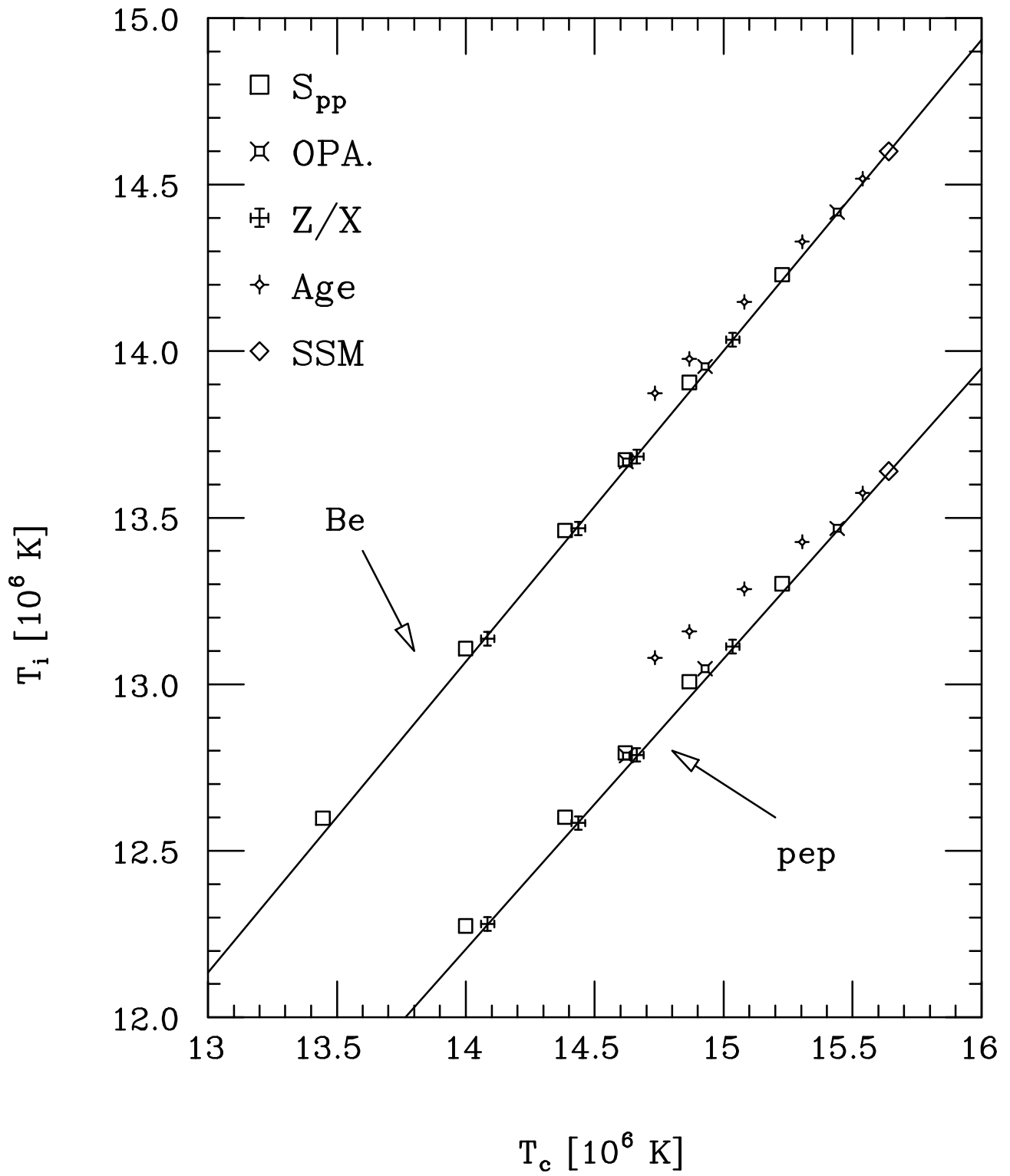


Fig. 13